SEDIMENTOLOGY the journal of the International Association of Sedimentologists

Sedimentology (2022) **69**, 1816–1840 doi: 10.1111/sed.12972

Instant sedimentation in a deep Alpine lake (Iseo, Italy) controlled by climate, human and geodynamic forcing

WILLIAM RAPUC*, FABIEN ARNAUD*, PIERRE SABATIER*, FLAVIO S. ANSELMETTI†, ANDREA PICCIN‡, LAURA PERUZZA§, ANTOINE BASTIEN*, LAURENT AUGUSTIN¶, EDOUARD RÉGNIER**, JÉRÔME GAILLARDET†† and ULRICH VON GRAFENSTEIN**

**CNRS, EDYTEM, Université Savoie Mont Blanc, 73000, Chambéry, France (E-mail: william.rapuc@hotmail.fr)*

†Institute of Geological Sciences and Oeschger Centre for Climate Change Research, University of Bern, Baltzerstrasse 1+3, 3012, Bern, Switzerland

‡Regione Lombardia, D.G. Territorio e Urbanistica, Struttura Sistema Informativo Territoriale, 20124, Italy

§Istituto Nazionale di Oceanografia e di Geofisica Sperimentale—OGS, Borgo Grotta Gigante 42/c, Sgonico, 34010, Italy

¶Division technique de l'INSU, CAROTTAGE - CONTINENTAL- FRANCE, UPS855, CNRS, ZP de Brégaillon CS 20330, La Seyne-sur-Mer, 83507, France

***LSCE, Commissariat à l'Energie Atomique–CNRS, Université de Versailles Saint-Quentin, Gif-sur-Yvette, 91198, France*

††Institut de physique du globe de Paris, CNRS, Université de Paris, Paris, F-75005, France

Associate Editor – Kyle Straub

ABSTRACT

The sedimentary processes in the deep basin of large peri-Alpine lakes have not been studied much on long timescales due to high coring complexity of such lake systems. In 2018, a 15.5 m long sediment section was retrieved from the deep basin of Lake Iseo (Italy) at 251 m water depth. A seismic survey associated with a multi-proxy approach using sedimentological and geochemical analyses, reveals that event deposits correspond to 61.4% of the total sedimentation during the last 2000 years. The great heterogeneity of textures, colours and grain-size distribution between the different types of event layers can be explained by the high number of potential sources of sediment in this large lake system. By combining a proxy of sediment sources with proxies of transport processes, flood events were distinguished from destabilizations of the slopes and the main delta. The three thickest mass wasting deposits correspond to major regional earthquakes events of 1222 CE, 1117 CE and around 700 CE. From a thorough comparison with regional climatic fluctuations and human activities in the watershed, it appears that periods of high sediment remobilization can be linked to a preceding increase in erosion in the watershed mainly under human forcing. Hence, even in large catchments, human activities play a key role on erosion processes and on sediment availability, disrupting the recording of extreme events in lacustrine archive.

Keywords Earthquake records, erosion, flood frequency, human activity, lake sediment.

INTRODUCTION

Several studies based on natural archives have recently shown how much human activities have played a key role upon erosion and sediment transport processes throughout the Holocene and more particularly over the last two millennia (Edwards & Whittington, 2001; Fuchs, 2007; Giguet-Covex *et al.*, 2012; Dotterweich *et al.*, 2013; Doyen *et al.*, 2013; Simonneau *et al.*, 2013; Zádorová *et al.*, 2013; Silva-Sánchez *et al.*, 2014; Arnaud *et al.*, 2016; Brisset *et al.*, 2017; Giosan *et al.*, 2017; Francke *et al.*, 2019; Rapuc *et al.*, 2019, 2021a; Walsh *et al.*, 2019). Indeed, the expanse of grazing and agriculture, as well as the deforestation that often accompanied them, may trigger a general destabilization of slopes and an increase in sediment flux towards depositional sinks (Edwards & Whittington, 2001). In European Alps, human activities have increased erosion from the end of the Neolithic (*ca* 4 kyr BP) and even more significantly at the beginning of the Iron Age and during the Roman Period (Giguet-Covex *et al.*, 2011; Simonneau *et al.*, 2013; Vannière *et al.*, 2013; Joannin *et al.*, 2014; Bajard *et al.*, 2016; Rapuc *et al.*, 2018, 2021a; Regattieri *et al.*, 2019; Andrič *et al.*, 2020). Even if lake sediments provide a continuous and well-preserved natural archive of such variations, strong and sudden inputs of sediment can disturb this record. Indeed, sediment availability in small lake basins and watersheds plays a key role in the sensitivity of the lake to record extreme events such as floods, avalanches or earthquakes (Wilhelm *et al.*, 2016; Brisset *et al.*, 2017; Fouinat *et al.*, 2018; Rapuc *et al.*, 2018). Human-triggered soil destabilization may lead to an apparent increase in flood frequency by increasing the amount of sediment available for erosion (Giguet-Covex *et al.*, 2012; Brisset *et al.*, 2017; Fouinat *et al.*, 2017). Whether it is climate-triggered or human-triggered, a rise in erosion results in increasing sediment fluxes which makes steep lake flanks, in particular in its delta area, much less stable, increasing the sensitivity of lake sediment to record the occurrence of earthquakes (Wilhelm *et al.*, 2016). By modifying the cycles of erosion and sediment transport processes, human activities hence impact the sedimentation in the different sinks.

However, previous studies were led in small-scale lakes and catchment areas. Very few investigations were conducted in large peri-Alpine lowland lake basins fed by large catchment areas, although such lakes are particularly promising targets to reconstruct past hydroclimate changes at a regional scale (e.g. Wessels, 1998; Wagner *et al.*, 2008; Arnaud *et al.*, 2016). Compared to smaller water bodies, large lakes are challenging to study due to: (i) the multiple sediment sources linked to multiple inflows; (ii) an inhomogeneity of the in-lake biogenic sedimentation at different water depth and location; and (iii) several processes that can impact the background sedimentation such as floods or earthquakes (Sturm & Matter, 1978; Sauerbrey *et al.*, 2013); making more difficult the interpretation of the erosion signal. It is also very challenging to recover a pluri-millennial sediment sequence in those lakes that are very often deeper than 100 m and where the total Holocene sediment accumulation often exceeds 20 m and sometimes 50 m.

Here, thanks to a new coring system, this study presents a novel approach with a long sediment core from a large peri-Alpine lake sampled in the deep basin of Lake Iseo at the downstream end of the Val Camonica valley in northern Italy. In this region, human activities are well-documented in the Val Camonica (e.g. Anati & Cittadini, 1994; Gehrig, 1997; Marziani & Citterio, 1999; Pini, 2002; Pini *et al.*, 2016) and various regional palaeoclimate records already exist (e.g. Büntgen *et al.*, 2011, 2016; Vannière *et al.*, 2013; Wirth *et al.*, 2013b; Joannin *et al.*, 2014). The main objective of this study was to identify the main sedimentary processes in such deep Alpine lakes under Geodynamic, Human and Climate forcing. A multi-proxy approach, combining a seismic survey with sedimentological and geochemical analyses, allows to document that the fluctuations in numbers and intensities of these events (floods and earthquakes) are related to sediment availability in the deep basin and in the lake catchment.

Study site

Lake Iseo (45°44.205′N; 10°4.340′E) is located in Lombardy, North of the Po Plain (Fig. 1A), at the southern end of the Val Camonica valley at an altitude of 185 m a.s.l. (above sea level). Lake Iseo (Latin name 'Sebino') is, with a length of 25 km and a surface area of 60.9 km^2, the smallest of the four major Italian peri-Alpine lakes. The depression that hosts the lake is a former Miocene canyon that was reshaped and re-eroded by several glacier advances and retreats during the Pleistocene epoch. Its current infilling is assumed to have been set since the last post-Late Glacial

Maximum retreat (Bini *et al.*, 1978). Lake Iseo is currently meromictic (Salmaso *et al.*, 2003; Ambrosetti & Barbanti, 2005). The last observed complete mixing of the deep water occurred in the 1980s (Salmaso *et al.*, 2003). From then, oxygen concentrations have continuously decreased within the deep water and conditions of permanent anoxia developed during the 1990s. Instrumental data provided by ARPA (Regional Agency for the Protection of the Environment, http://arpalombardia.it/) indicates that the limit of the depth of the hypolimnion varies between 80 m and 100 m. At these depths, the oxygen saturation and pH values decrease sharply, while dissolved calcium concentrations increase.

Lake Iseo bathymetry shows two sub-basins separated by Monte Isola (Fig. 1B). The smaller basin, Sale Marasino Basin, is 100 m deep and disconnected from the main basin and from the sediment input of the Oglio river by the Monte Isola plateau in its northern part. The Holocene sedimentation of this area was already studied (Lauterbach *et al.*, 2012; Rapuc *et al.*, 2019). The main basin is however much deeper (251 m) and had never been cored. It is located north-west of Monte Isola (Fig. 1B) and is protected from underflows coming from all the inlets located in the Marone delta or feeding Monte Isola Plateau and the Sale Marasino Basin by the presence of a ridge north-west of Monte Isola (Fig. 1B).

The Oglio river, originates from the Adamello Massif. It is the main tributary and the outlet of Lake Iseo (Fig. 1B). This river drains a relatively large watershed (1842 km^2) with a maximum elevation of 3539 m a.s.l in the Adamello Massif, in the northern part of Val Camonica and a mean altitude of 1400 m a.s.l (Garibaldi *et al.*, 1999). The watershed of Lake Iseo extends up to 60 km northward into the Val Camonica valley and only several kilometres to the east and west of the lake. It is mainly composed of Triassic, Jurassic and Cretaceous limestones and marlstones in the southern part, with some outcrops of Permian sandstones. In the northern part of the Val Camonica, metamorphic rocks linked to the Alpine orogeny with Tertiary tonalites, granodiorites and quartzodiorites are cropping out. Glaciers and rock glaciers are present in the north-eastern part of the watershed (Scotti *et al.*, 2013). The Val Camonica is well-known for its abundance of rock carvings that are registered on the UNESCO World Heritage List (Ruggiero & Poggiani Keller, 2014). This archaeological evidence provides indications of human presence in the Iseo region since the Mesolithic period (9 to 6 kyr BC) and agro-pastoral practices as early as 6.5 kyr BP.

The Val Camonica valley and more broadly the north-eastern part of the Italian Alps are affected by a moderate to high seismic hazards (Stucchi *et al.*, 2004; Giardini *et al.*, 2013; Wiemer *et al.*, 2015; Pagani *et al.*, 2018). The tectonic setting is the result of complex collisional and post-collisional phases of the Alpine orogeny (Dal Piaz *et al.*, 2003). The current crustal shortening in the area is estimated to *ca* 1 mm $year^{-1}$ (Serpelloni *et al.*, 2005), and several devastating earthquakes have been recorded in the last millennium (Fig. 1A; for the most updated Italian earthquake catalogue see Rovida *et al.*, 2019, 2020). The local seismic activity (magnitude $M < 6$) is ascribed to fold-and-thrust systems, mainly west–east oriented, blind faults towards the Po Plain, and north–south oriented in the Garda Lake area (Livio *et al.*, 2009; DISS Working Group, 2018).

MATERIALS AND METHODS

Seismic survey

Two previous studies were made on sediment cores from Lake Iseo (Fig. 1B), retrieved from the Sale Marasino isolated basin (SEB05 and SEB06) and the Monte Isola Plateau (SEB10), which separates the Sale Marasino Basin from the main Iseo Basin that is fed by the Oglio river. Hence, none of those sites receives any

Fig. 1. Lake Iseo location and settings. (A) Location of Lake Iseo (Italy), its watershed (red dashed line) and different lakes of the Italian southern Alps: Lake Como, Lake Garda, and Lake Ledro. The orange and yellow stars correspond to the location of historic earthquakes with a Magnitude ≥6 and <6, respectively. (B) Lake Iseo Bathymetric map associated with the description of the different morphological features and the different coring sites. Seismic profiles west–east (C) and south–north (D) oriented across the deep basin showing the coring site location (vertical red line) and the principal generations of mass wasting deposits (MWD, coloured lines). The depth of the seismic profile is expressed in metres below lake surface (m b.l.s.), assuming a mean P-wave velocity of 1450 m s^{-1} in water and sediments.

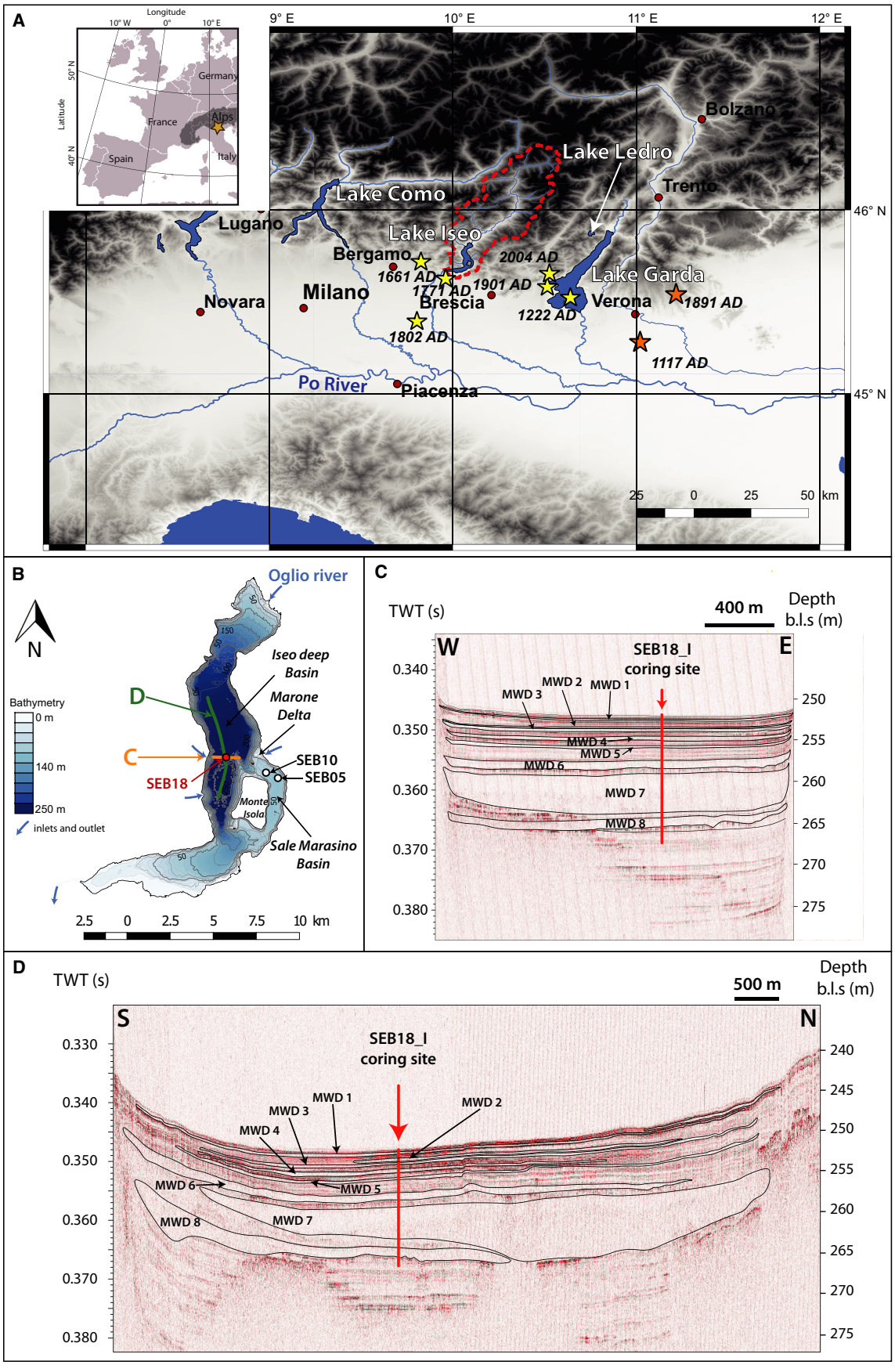

sediment input from the Oglio river (Lauterbach *et al.*, 2012; Rapuc *et al.*, 2019). A seismic reflection survey was conducted in the deepest basin in July 2018 to select a suitable coring site, minimizing the amount of reworked sediment and presenting the thinnest mass wasting deposits (MWD). For this survey, *ca* 51 km of 3.5 kHz pinger (Geoacoustics Limited, Yarmouth, UK) single-channel data were acquired with a shooting interval of 500 ms and recorded the SEG-Y data with a sample frequency of 24 kHz. A bandpass filter (1500 to 6500 Hz) was applied. The coring location, SEB18_I (45°43.536'N; 10°3.888'E), was selected in the centre of the deep basin at the intersection of two perpendicular seismic lines, north-west of Monte Isola by 251 m water-depth (Fig. 1B). This area is protected from the Marone delta sediment input by the ridge north-west of Monte Isola and is supposed to be only influenced by the sediment input from the Oglio river and from small gullies and tributaries coming from the hills, west of the coring site.

Coring, and lithological description

In October 2018, 39.2 m of sediment was retrieved (Fig. S1) from six different holes in close vicinity (<20 m). For this survey, two UWITEC 90 mm diameter piston corers (Uwitec, Mondsee, Austria) were used, the pushing power was provided using a semi-manual UWITEC downhole hammer, operated from a UWITEC platform (EDYTEM/LSCE/C2FN). Two metres-long sections from the different holes were taken with a 1 m offset to ensure a sufficient overlap in order to provide a continuous record (Fig. S1). Most of the sections were split, photographed at high-resolution (20 pixels mm^{-1}), described and logged in detail using the Munsell colour chart. The identification of specific layers on the overlapping sections combined with correlations of XRF-core scanner signals allowed the creation of a 15.5 m long composite sediment sequence (hereafter called SEB18, Data S1). One gap occurs in the sequence from 1342.4 to 1362.4 cm: between two sections where an overlapping section is missing. While describing the core sections, specific attention was given to the identification of layers interbedded within the background sedimentation. These event layers were visually documented, described, measured and logged.

Loss on ignition

Loss on ignition (LOI) analysis was conducted to estimate the organic matter and carbonate content throughout the sediment sequence. Because many layers interrupt the sediment section, a 10 cm evenly spaced discrete sampling step was applied on the background sedimentation to perform LOI following the protocol that was defined by Heiri *et al.*, 2001. Several discrete samples were also collected in the main event layers. Before the LOI analysis, the dry bulk density (DBD) was calculated from the samples by performing a constant volume sampling and by weighting the sediment after 72 h of drying at 60°C. Then, the sediment samples were crushed before being heated in a muffle furnace at 550°C for 4 h and at 950°C for 2 h. The relative weight loss during the first (hereafter, LOI550) and second heating phases (hereafter, LOI950) corresponds to the fractions of organic matter and of carbonate, respectively. Finally, the non-carbonate ignition residue (NCIR) was obtained by removing LOI550 and LOI950 from the initial dry weight. Percentages obtained for LOI550, LOI950 and NCIR present standard deviation of 0.91 (Rapuc *et al.*, 2021a).

Geochemical analyses

To characterize variations of major elements, X-ray fluorescence (XRF) geochemical analyses were performed on the EDYTEM laboratory's AVAATECH Core Scanner (Avaatech XRF Technology, Alkmaar, The Netherlands) throughout the SEB18 sediment sequence. A continuous 5 mm step measurement was applied with two runs: one at 10 kV and 0.3 mA for 30 s, to detect lightweight elements, such as Al, Si, K, Ca and Ti; and a second run performed at 30 kV and 0.4 mA for 40 s, to detect Mn, Fe, Br, Rb, Sr and Zr. The XRF core-scanning results are expressed hereafter as count per second (cps) within each element-attributed X-ray fluorescence energy range. Mean analytical errors and mean standard deviation are presented hereafter and are lower than 10% of the total signal for every element: Al (126 cps, SD = 1%), Si (321 cps, SD = 0.3%), K (329 cps, SD = 0.5%), Ca (614 cps, SD = 0.17%), Ti (227 cps, SD = 1.3%), Mn (118 cps, SD = 1.3%), Fe (627 cps, SD = 0.1%), Br (227 cps, SD = 10.7%), Rb (328 cps, SD = 2.0%), Sr (389 cps, SD = 1.1%) and Zr (398 cps, SD = 3.1%). To identify principal sediment end-members and correlations between

the detected elements, a principal component analysis (PCA) on centred data was conducted on the whole XRF dataset (Sabatier *et al.*, 2010) using 'FactoMineR' package on the R software (The R Foundation).

Chronology

On SEB18 sediments, an age-depth model was built by combining varve counting, short-lived radionuclides (^{210}Pb, ^{137}Cs and ^{241}Am) and ^{14}C along the 15.5 m of the composite section (Rapuc *et al.*, 2021a). Varves were counted on the first 37 cm of SEB18_I_Pil02 section. Then, 38 samples were collected over the first 48.1 cm of the sequence to measure short-lived radionuclide activities at the Laboratoire Souterrain de Modane using the well-type germanium detectors (Reyss *et al.*, 1995). Short-lived radionuclide chronology was carried out using R code package 'serac' (Bruel & Sabatier, 2020). Thirteen samples of vegetal macro-organic remains were used to perform ^{14}C measurements at the LMC14 laboratory (CNRS). Dates were calibrated at 2-sigma using the Intcal20 calibration curve (Reimer *et al.*, 2020). Rapuc *et al.* (2021) used the R code package 'clam' (Blaauw, 2010) to compute the age-depth model of the non-event sections.

RESULTS

Seismic imagery

Assuming a P-wave velocity (Vp) of 1450 m s^{-1}, the seismic signal penetrated 25 to 30 m of sediment below the lake floor. In areas where free gas occurs, particularly near deltas where a high amount of organic matter is buried, penetration is less, and characteristic high-amplitude anomalies occur that mark the gas front (Fig. 1C and D). The seismic facies comprise sections where seismic reflectivity is high and subparallel reflections with high lateral continuity occur; these are interpreted as regularly stacked background sedimentation. The associated reflections all onlap the steep lateral sides of the lake basin. Intercalated within these reflective sections, several transparent to chaotic deposits typical of mass-wasting deposits (MWD) (e.g. Strasser *et al.*, 2013; Chapron *et al.*, 2016) interrupt the background sedimentation. They often show high amplitude reflections at their bases. The upper part of these MWDs is usually transparent, indicating a megaturbidite/homogenite unit representing the latest stage of event sedimentation when the fine particles eventually settle. The lower parts of MWDs may show some internal architecture with reflections indicating various basal flow units. Some of the MWDs show a mound-like geometry with larger thickness in the centre of the basin (Fig. 1D). At least eight MWDs are identifiable across the deep basin of Lake Iseo, with three deposits presenting a metric thickness (Fig. 1C and D). Most of these deposits seem to cover the entire basin and, considering their geometry, appear to originate from its southern or northern part.

The three thickest MWDs are labelled MWD6, MWD7 and MWD8 (Figs 1C, 1D and 2). Interpolation of their thicknesses over the whole basin result in volume estimates of 11×10^6 m^3 for MWD6, and a combined 89×10^6 m^3 volume calculated for both MWD7 and MWD8 because they are stacked and therefore hard to subdivide on the seismic data.

Sedimentology

Lithologies and stratigraphic units

Background sedimentation occurs in 39% of the SEB18 sediment section. This sedimentation is visually distinguishable from homogeneous or graded layers interpreted as event layers and accounting for 61% of the total accumulation. Within the background sedimentation, two stratigraphic units can be distinguished (Fig. 2): Unit I (0 to 32.3 cm) is composed of dark grey clay becoming greenish at the base of the unit. It is composed of thin alternations of light greyish olive clayey (10Y 6/2), grey (5Y 5/1), pale yellow (5Y 7/3) and/or dark laminae (5Y 2.5/1). Fifty-eight laminae successions were counted in this unit that also includes several graded layers. This unit coincides with the varved organic gyttja which has already been described in cores retrieved in Lake Iseo (Lauterbach *et al.*, 2012; Rapuc *et al.*, 2019) and related to the recent eutrophication period of Lake Iseo. LOI was not measured in this unit.

In Unit II, from 32.3 cm to the bottom of the core (1550.9 cm), the background sedimentation of the SEB18 sedimentary section is composed of grey clay (10YR 5/1) featuring dark spots that disappear after oxidation. The LOI550 ranges between 3.8% and 7.5%, with a mean value of 5.3%. The LOI950 ranges between 5.7% and 18.2% with a mean value of 12.2%. The background sedimentation of Unit II is interrupted by numerous graded layers that are described

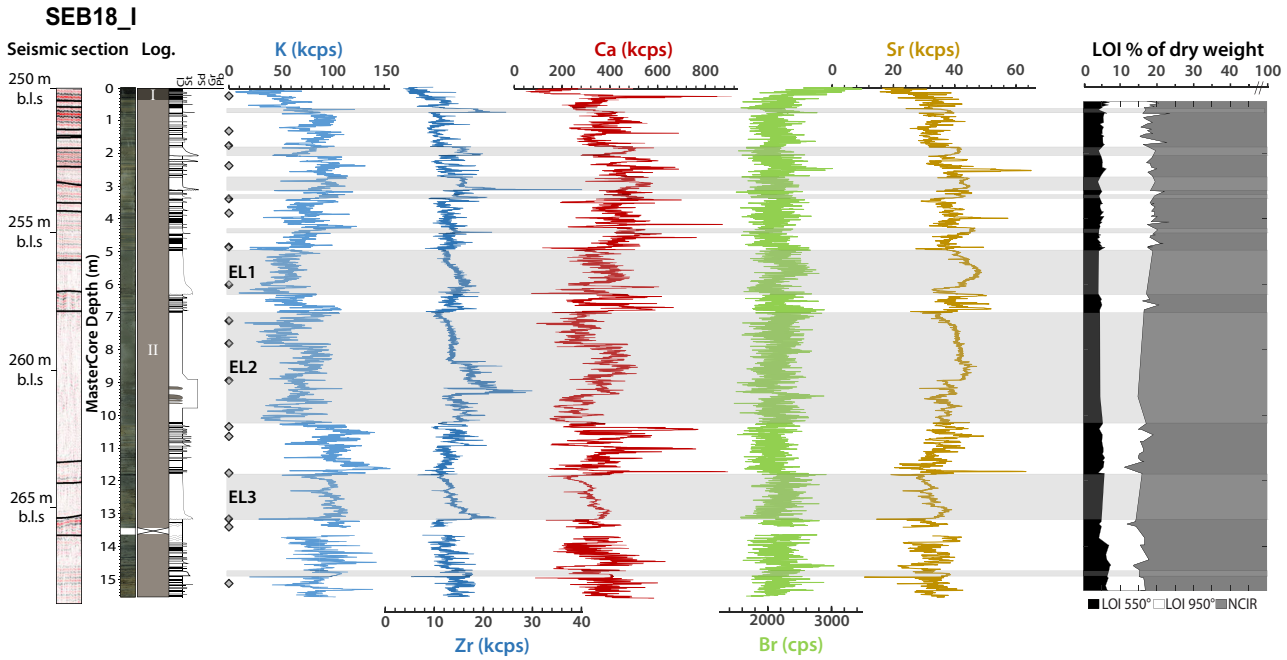

Fig. 2. Sedimentological and geochemical data. A close-up view of the seismic profile (Fig. 1C) section is compared with lithological and geochemical data. A core image of the 15.5 m of the SEB18 sediment sequence and stratigraphic units are associated with the grain-size sensitive lithological column, selected geochemical results (K, Zr, Ca, Br and Sr contents) and loss on ignition (LOI). The depth of the seismic section is expressed in metres below lake surface using a Vp of 1450 m s^{-1} and is scaled approximately to fit the length of the sediment core. Grey shading represents the thickest graded layers. Grey diamonds represent the junction between the different sections of SEB18 sediment sequence.

below. The grain size of the background sedimentation is largely dominated by fine silts and clays (Q90 <20 μm).

Event layers

Event layers were macroscopically identified and counted. Their colours vary from dark grey to light brown (2.5Y 5/2), very dark greyish brown (10YR 3/2), dark grey (10YR 4/1) and black (10YR 2/1). These layers either have a normally graded upward-fining grain-size pattern like turbidite type deposits or they display homogeneous lithologies termed 'homogenites' (Kastens & Cita, 1981; Hieke, 1984). Because they interrupt the background sedimentation, they are considered as instantaneous event layers. Thickest layers present fine to medium sand at their bases (Q90 >200 μm). Most of the layers are thin (i.e. below 1 cm), but three of them are complex sequences that are more than 1 m thick: (i) Event layer 1 (EL1) is comprised between 493.5 cm and 626.1 cm, i.e. 1.32 m thick; (ii) Event layer 2 (EL2) is 3.37 m thick and located between 682.3 cm and 1020 cm; and (iii) Event layer 3 (EL3) is comprised between 1178.5 cm and 1320.7 cm, i.e. 1.42 m thick (Fig. 2). EL1 and EL3 present a fine graded sandy base followed by a thick homogeneous layer, composed of very fine sand to silt and a thin dark clayey top. EL2 is the thickest sequence interbedded within the SEB18 sediment pile. It presents a lower part made of medium to fine sand associated with mud-clasts. This is followed by homogeneous silts from 891.5 to 683.7 cm and a thin clayey top. EL1, EL2 and EL3, similar to most of layers thicker than 5 cm, present an erosive base. The three thickest layers are also identifiable on the seismic profiles (Figs 1C, 1D and 2) as they are correlated to MWD6, MWD7 and MWD8, respectively, and seem to originate from the Oglio delta in the northern part of the deep basin. A total of 146 ≥ 1 mm layers have been identified and measured for thickness (average thickness: 6.5 cm; median thickness: 1.2 cm).

Geochemical analyses

Unit I shows low values of K (<70 kcps), of Zr (<10 kcps with only one peak at 15 kcps) and an upward increase of the Br values to the top of

the unit (from 2000 to 3000 cps). In the background sedimentation, the Zr and K signals increase downcore (Fig. 2) towards the base of the sediment sequence (Unit II). No clear trend is visible for other elements, as Ca, Br and Sr display relatively constant values. Several event layers present a peak of Zr at the base and an increase of K value towards the top (Fig. 2). Bromine and calcium are very variable and fluctuate within the event layers, while Sr shows low variability. The samples that were collected in these thickest event layers for LOI550 and LOI950 measurements did not present significant changes compared to others. Individual and variables factor maps were obtained from a PCA conducted on the XRF data (Fig. 3). These biplots highlight the geochemical distribution within the two different sedimentary units and the relationships between the different elements. Dimensions 1 and 2 (denoted as Dim1 and Dim2) represent 52.7% of the total variability. Three chemical end-members were identified from the variables factor map. The first one is positively correlated with Dim1, yields high positive loadings for the major terrigenous elements (Al, Si, K, Ti, Rb and Fe), and is thus denoted as 'terrigenous'. The second end-member, shows negative loadings on Dim2 and allows the discrimination of Br, Mn and Pb. Bromine was previously correlated in other cores of the same lake to organic matter content and Mn to oxygenation processes in the lake (Rapuc *et al.*, 2019), Pb is probably complexed with organic matter. This pole is then denoted as 'organic matter-related elements'. The third end-member, shows positive correlation with Dim2 and yields high positive values for Zr, Ca and Sr. Strontium is usually present in marine limestone, which constitutes a major part of the watershed's outcrops. Zirconium is generally associated with coarse grain size explaining the peak at the base of each thick coarse graded layer. Thus, this end-member is interpreted as representative of the carbonates and coarsest terrigenous inputs from the watershed, characterized by the presence of reworked marine carbonates (Ca and Sr) and heavy minerals (Zr). It is thus denoted as 'coarse terrigenous fraction'.

To understand the specificity of the two stratigraphic units and the different event layers, an individual factor map was drawn (Fig. 3B). From this map, Unit I is negatively correlated with the terrigenous end-member and positively with the organic matter end-member. This confirms its important organic content already observed in other cores

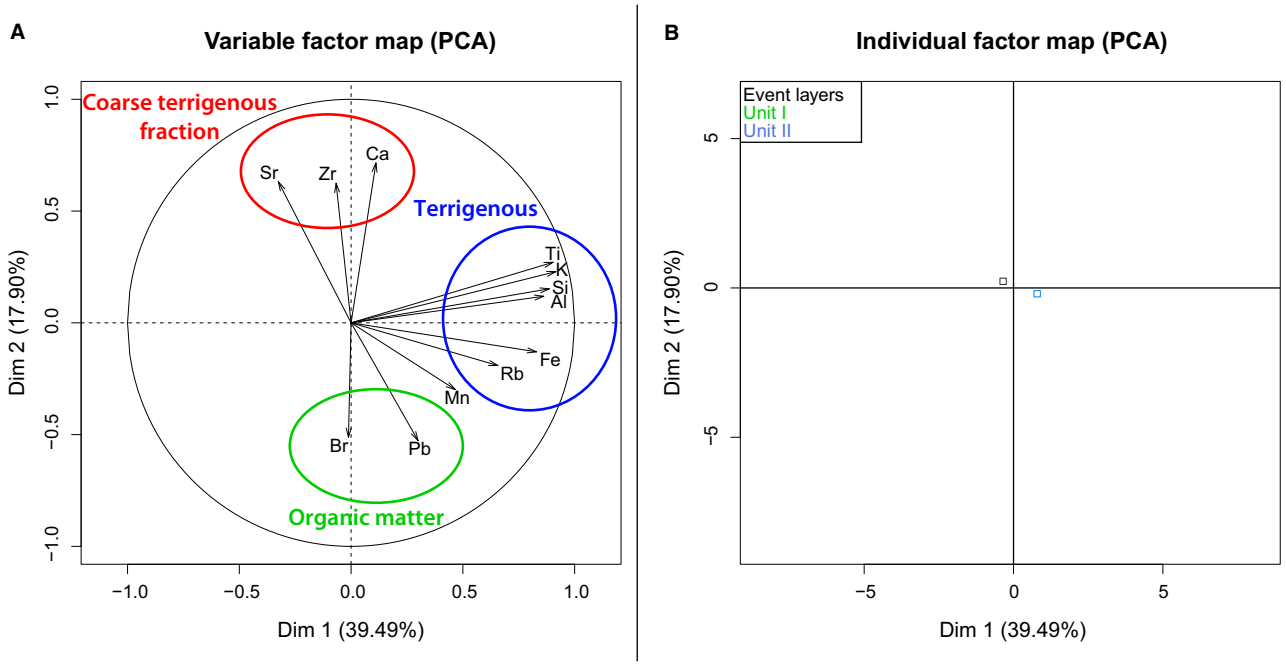

Fig. 3. Variable and individual factor maps from the principal component analysis (PCA). (A) Variable factor map with three end-members (terrigenous, organic matter and coarse terrigenous fraction linked to carbonates). (B) Individual factor map with the two sedimentological units added as an illustrative variable and compared with the event layers.

from Lake Iseo (Lauterbach *et al.*, 2012; Rapuc *et al.*, 2019). Unit II presents a large variability but is positively correlated with the terrigenous end-member and is also characterized by low Ca, Zr and Sr. The event layers present a wide distribution on the individual factor map but are characterized by relatively low organic matter content. The PCA analyses and XRF data did not allow to directly classify event layers into different types.

Chronology

Short-lived radionuclides and varve counting

From the first 37 cm, 58 varve couplets were identified and counted, yielding a mean sedimentation rate of *ca* 5.3 mm year^{-1} including event deposits (Fig. 4A). This counting allows to assign the earliest varve to 1960 CE corresponding to the beginning of the eutrophication of the Monte Isola Plateau, already established by varve counting from the SEB10 sediment sequence (Rapuc *et al.*, 2019). This timing is almost identical to that observed in Lake Varese, in northern Italy (Bruel *et al.*, 2018). The age of the uppermost turbidite matches with a well-documented flood event that occurred in 1994 CE (Luino *et al.*, 2002; Guzzetti & Tonelli, 2004).

The ^{210}Pb excess profile ($^{210}Pb_{ex}$) profile shows a regular decrease (Fig. 4A) from 470 mBq g^{-1} to low activities (<30 mBq g^{-1}) punctuated by distinct drops. Following Arnaud *et al.* (2002), these low values of ^{210}Pbex corresponding to event deposits were excluded from the construction of an event-free sedimentary record as they were considered as instantaneous. This study uses a logarithmic scale to plot $^{210}Pb_{ex}$ event free data and to underscore a single-point alignment that indicates a constant sedimentation rate of 4.41 ± 0.06 mm year^{-1} (R^2 = 0.88) for the uppermost 48 cm thanks to the Constant Flux Constant sedimentation model (Bruel & Sabatier, 2020).

The ^{137}Cs profile shows a clear peak between 16.7 cm and 19.7 cm with a maximum activity (>1300 mBq g^{-1}) at 18.7 cm; this peak is associated with a peak of ^{241}Am (>2.3 mBq g^{-1}) and is widely attributed in the literature to nuclear fallout from the 1986 CE Chernobyl accident (e.g. Appleby *et al.*, 1991). The ^{241}Am profile presents a peak (>2.2 mBq g^{-1}) at 43.5 cm with a peak in the ^{137}Cs (>97 mBq g^{-1}) profile between 42.5 cm and 43.5 cm. These peaks correspond to the maximum nuclear weapon tests at 1963 CE (Appleby *et al.*, 1991). The 1986 CE peak is in good agreement with the sedimentation rate that was derived from the $^{210}Pb_{ex}$ profile and the varve counting. The $^{210}Pb_{ex}$ profile presents an offset from the 1963 CE peak, probably due to a change in the sedimentation rate around 40 cm. These chronological markers were added into the age-depth model to constrain it for the upper portion of the sediment section.

Carbon-14 and age-depth model

Thirteen samples of terrestrial macro-remains were analysed to provide radiocarbon ages. Once calibrated, four of these 13 dates (Table 1) were not used because they presented ages older than the best-fit age-depth curve of the SEB18 sequence. These four ages were consistently sampled from the top of detrital event layers: these macro-remains are interpreted as originating from previously deposited sediment in the lake.

The thickness of each layer was subtracted from the SEB18 sediment sequence depth to create an event-free depth (Fig. 4B) and to obtain the best age-depth model. This study used the combination of varve counting and the nine remaining calibrated ages to generate the age-depth model with a smooth spline model with 0.4 for the smooth parameter. The sedimentation rate presented hereafter (Fig. 4C) was calculated from the event-free depth and is not influenced by the variation of the event layer occurrence. To provide a date for all event layers, all event layers were reintegrated to the age-depth model (Fig. 4D).

The SEB18 sequence covers the last 2000 years (21 to 2018 CE) with a background sedimentation rate that varies between 5.1 mm year^{-1} and 2.1 mm year^{-1} with a mean of 3.1 mm year^{-1}. Three periods of gradual increase of sedimentation rate are identified (Fig. 4C) in the sequence. The first one occurs between 500 CE and 800 CE with a maximal sedimentation rate of 3.2 mm year^{-1}. After a small decrease until approximately 900 CE (2.7 mm year^{-1}), the sedimentation rate increases gradually and presents high values (3.06 mm year^{-1}) between 1000 CE and 1400 CE. From 1500 CE towards the top, the sedimentation rate increases sharply and reaches its highest value of 5 mm year^{-1}.

INTERPRETATION AND DISCUSSION

Provenance of background sedimentation

On average, LOI analyses indicate that organic matter accounts for 5.3% of the background

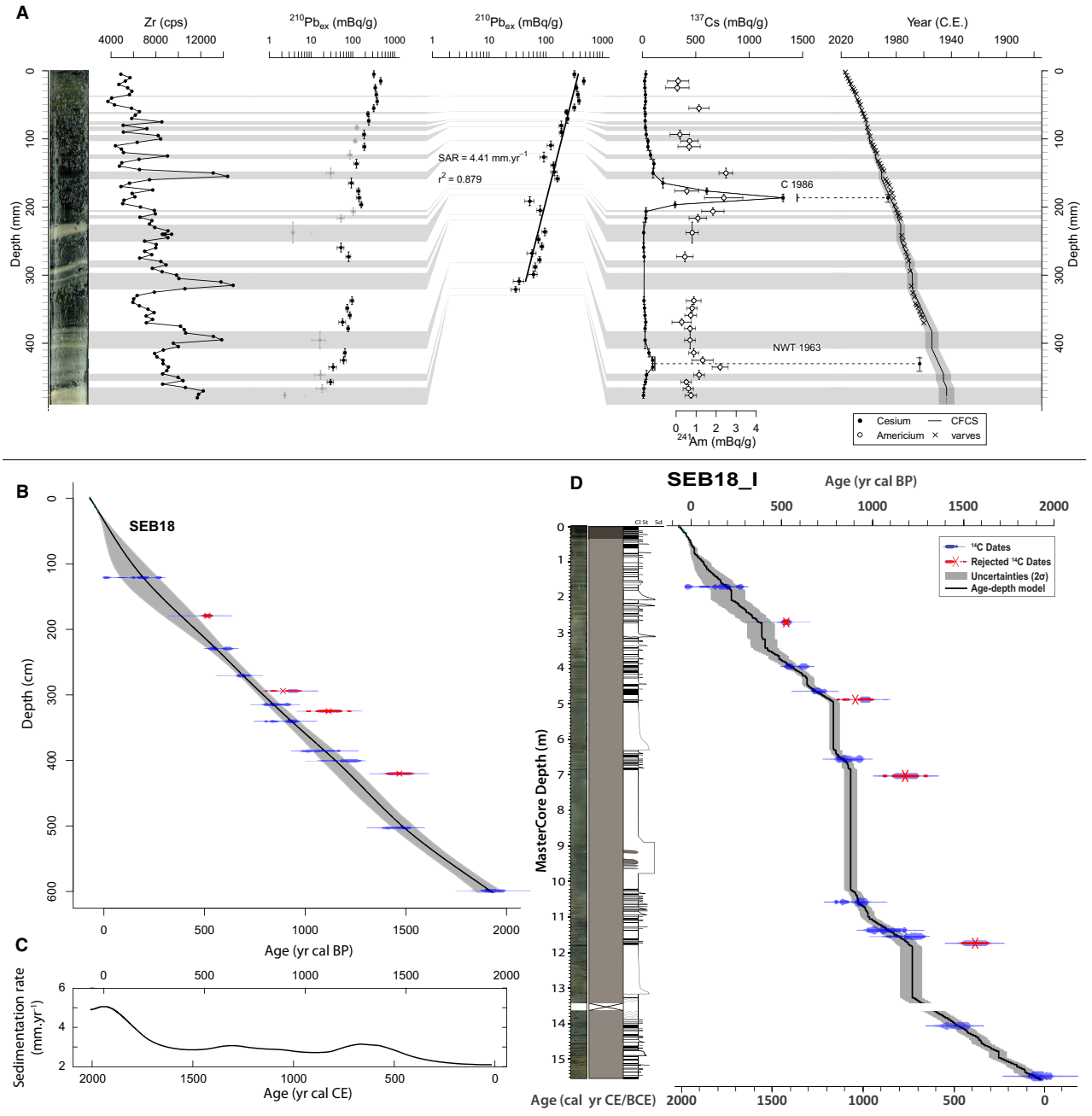

Fig. 4. Age-depth models. (A) Short-lived radionuclide data: $^{210}Pb_{ex}$ in logarithmic scale associated with the ^{241}Am and ^{137}Cs profiles with the picture of the top 48 cm of SEB18 sequence. (B) Age–depth model in event-free depth. (C) Sedimentation rate (without event layers) obtained from the age-depth model, (D) Complete age-depth model associating radiocarbon and varve counting.

sedimentation, whereas carbonates represent 12.2%. Hence, most of this sedimentation is made of siliciclastic material (Fig. 2). As Lake Iseo is a temperate hardwater meromictic lake, where the deep water does not mix every year (Garibaldi *et al.*, 2003), it is assumed that calcite precipitates in the lake as is the case worldwide for this lake's type (Küchler-Krischun & Kleiner, 1990). The ARPA instrumental data indicate that pH values decrease sharply between 80 m and 100 m b.l.s. at the upper limit of the hypolimnion (Fig. 5A). This is accompanied by

Table 1. Radiocarbon ages for the SEB18 sediment sequence. Event-free depth was calculated by excluding the thicknesses of each graded bed considered as event layers. Samples in bold correspond to dates excluded from the age-depth model (Fig. 4B and C).

Sample name	Core	Depth (cm)	Event-free depth (cm)	Radiocarbon age	Age cal yr BP 2 σ range	Type
SAC-A 57155	SEB18_I_C_01A	169.8	120.8	170 ± 30	−3 to 289	Stem
SAC-A 57512	**SEB18_I_B_02A**	**271.8**	**179.3**	**465 ± 30**	**490 to 538**	**Plant debris**
SAC-A 57513	SEB18_I_C_02A	395.0	229.3	555 ± 30	520 to 639	Plant debris
SAC-A 57156	SEB18_I_B_03A	463.7	270.4	745 ± 30	662 to 726	Plant debris
SAC-A 57514	**SEB18_I_C_03A**	**488.2**	**294.0**	**1015 ± 30**	**802 to 978**	**Plant debris**
SAC-A 57157	SEB18_I_B_04A	653.2	314.7	950 ± 30	796 to 925	Plant debris
SAC-A 57515	**SEB18_I_C_04A**	**702.9**	**324.9**	**1190 ± 30**	**1007 to 1226**	**Wooden debris**
SAC-A 57516	SEB18_I_B_06A	1058.7	340.2	1000 ± 30	799 to 966	Plant debris
SAC-A 57158	SEB18_I_C_06A	1136.4	385.4	1150 ± 30	980 to 1173	Plant debris
SAC-A 57517	SEB18_I_C_06A	1153.4	400.5	1255 ± 30	1085 to 1277	Plant debris
SAC-A 57518	**SEB18_I_B_07A**	**1183.4**	**420.2**	**1575 ± 30**	**1401 to 1535**	**Twig**
SAC-A 57519	SEB18_I_B_08A	1406.9	502.8	1550 ± 30	1379 to 1526	Plant debris
SAC-A 57520	SEB18_I_B_08B	1548.9	598.7	1980 ± 30	1876 to 1992	Plant debris

dissolved calcium concentration increase (Fig. 5B). Depending on the particle sizes and the settling times, some carbonate dissolution can occur at great depth in hard water lakes (Ramisch *et al.*, 1999). In Lake Lugano, another peri-Alpine lake, it has been shown that only calcite with a diameter larger than 40 μm reaches the lake bottom at 288 m (Ramisch *et al.*, 1999). Because authigenic carbonates in lakes have a low sinking velocity and usually present a diameter lower than 20 μm, as demonstrated in Lake Bourget (Arnaud, 2005), they are not likely to be preserved during their settling in the deep basin of Lake Iseo and are not supposed to contribute significantly to its background sedimentation. Then, fine-grained authigenic biogenic carbonates can only be preserved above a certain depth, where re-dissolution processes do not impact small sized particles: above the hypolimnion on slopes and plateau (Fig. 5C and D) presenting an inclination lower than the theoretical angle of repose of wet clayey material (>30°, Glover, 1997). In the Iseo deep basin, as settling times play an important role, most of the carbonate recorded in the background sedimentation is supposed to be linked to detrital inputs from the watershed through erosion of the limestone and marlstone bedrock, which is strongly suggested by the correlation between Ca, Sr and Zr (Figs 2 and 3A).

Oglio river waters and thus the sediment inflow by the Oglio plume are deflected towards the western shore of Lake Iseo due to the Coriolis influence (Pilotti *et al.*, 2013, 2018). In normal flow conditions (*ca* 50 m^3 s^{-1}; Groppelli *et al.*, 2011; Hogg *et al.*, 2013), the water underflow coming from the Oglio inlet only influences the first 100 m of depth of the lake basin, while the horizontal length of overflow intrusion is limited to 3 km (Hogg *et al.*, 2013). Thus, most sediment input from the Oglio river during normal flow conditions is accumulated close to the delta or on the north-western shores of Lake Iseo. Therefore, the input of detrital sediment in the deep basin is mainly related to flood events: when the current is strong enough, underflows can flow beyond the delta and lead to the settling of thin particles after the decrease of the turbiditic current in the deep basin. It is thus very likely that the background detrital sedimentation of the deep basin of Lake Iseo corresponds to the decantation of the end of underflows linked to minor flood events. A minority of this sedimentation can also be linked to gullies and small rivers from the hillslopes west and east of the deep basin.

Origin and trigger of the event layers

In large lowland lake systems, several mechanisms can trigger event layers, such as : (i) considerable lake-level fluctuations; (ii) autogenic destabilization of slopes and deltas due to sediment overloading; or (iii) to seismic shaking; and (iv) flood events (e.g. Sauerbrey *et al.*, 2013; Rapuc *et al.*, 2018). The present study found no historical evidence of significant fluctuations of the outflow level, thus, a lake level triggering

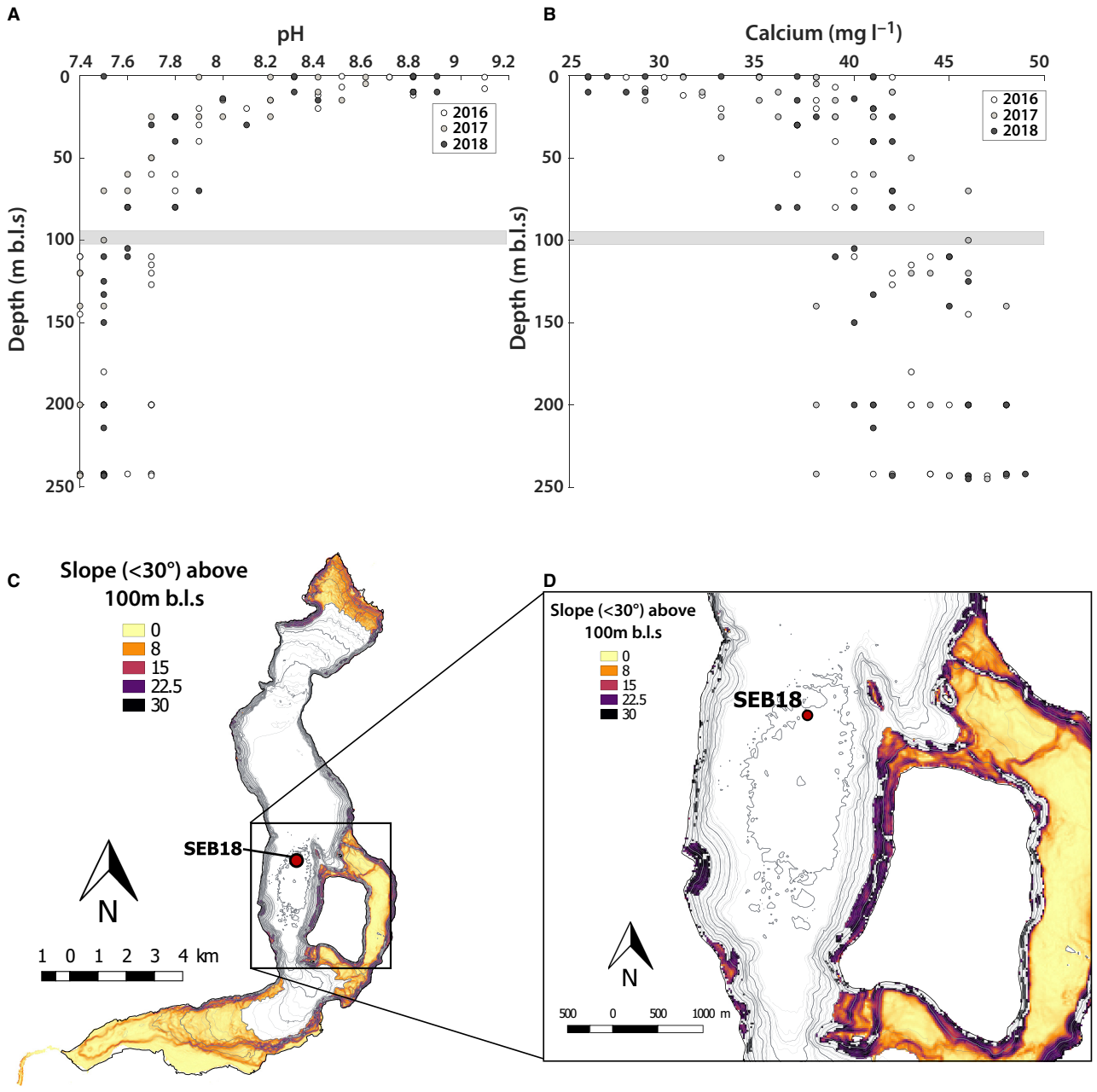

Fig. 5. pH (A) and dissolved calcium (B) profiles, recorded in the deep basin of Lake Iseo, close to the coring site, in 2016, 2017 and 2018 by ARPA (http://arpalombardia.it/). (C) Map presenting slopes of Lake Iseo with an inclination lower than 30° above 100 m b.l.s. where authigenic carbonates could accumulate (D) Close-up of map (C) in the deep basin around the coring site.

mechanism cannot be invoked to explain the thick layers recorded in the deep basin. Due to the high sedimentation rate recorded (Fig. 4C), sediment overloading on the lake slopes, on the delta of the Oglio, or on those of small tributaries are likely to induce MWD leading to the deposition of graded layers in the deep basin of Lake Iseo. Equally, this high sedimentation rate implies a high sensitivity of the lake to seismic shaking (Wilhelm *et al.*, 2016; Rapuc *et al.*, 2018). With a mean sedimentation rate of 3.06 mm year^{-1}, the probability for an earthquake to induce a MWD and related event layers in Lake Iseo is higher than in most previously

studied Alpine lakes (Wilhelm *et al.*, 2016). Moreover, such lake basins with sharp shelves and a flat lake floor provide typical settings for mass movements (Sauerbrey *et al.*, 2013).

In terms of flooding, as previously mentioned, most floods contribute to the background sedimentation in the deep basin of Lake Iseo with the distal low-velocity underflows reaching the coring site with the finest suspended particles. In contrast to these signatures in the background sedimentation, floods can also be recorded in the deep basin as event layers either when: (i) strong underflows linked to extreme flood events produce a current important enough to reach the deep basin and produce a turbidite layer distinguishable from the background sedimentation as for the 1994 CE event; or when (ii) flood events come from nearby tributary rivers. In summary, only two main mechanisms can be at the origin of the event layers recorded in the SEB18 sequence: (i) extreme flood events from the Oglio river or flood events from gullies and small tributaries coming from the western hillsides of the lake; and (ii) destabilizations of slopes and delta triggered by seismic shaking or sediment overloading.

In SEB18 sequence, 146 graded layers were identified and interpreted as event layers. Colours and textures from macroscopic observations, PCA and XRF alone were insufficient to distinguish and classify these layers and to link them to a specific triggering mechanism. This is probably due to the multiple provenances of sediment particles in the deep basin of Lake Iseo. Only a thorough knowledge of the functioning of the sedimentation in the lake, associated with a multiproxy approach, can help to disentangle the different origins of the sediment in event layers and allows the interpretation of their triggering mechanisms. To do so, it was necessary to identify the potential source areas and transport mechanisms of each event layer.

Locating potential source areas

It was assumed that there could be only two potential sources of sediment making the event layers: (i) detrital sediment from the Oglio river and/or delta; and (ii) sediment from lake slopes overhanging SEB18 coring site (lateral sources). To distinguish those source areas, the chemical composition and the thickness of event layers had to be considered together.

Indeed, whereas deltas are obvious sources of event layers, through stream flood and delta collapse, any sediment accumulation on slopes above SEB18 coring site could potentially slide down to the lake bottom, if it is thick enough. A thick accumulation is less likely to occur on slopes >30° in the absence of progradation processes (Adams *et al.*, 2001, and references therein). Moreover, in the absence of major terrigenous input such accumulation should be made of in-lake produced biogenic compounds. If such a source exists it hence requires to present a slope <30° and be favourable for biogenic matter accumulation, which in hard-water lakes is mainly made of calcite (e.g. Küchler-Krischun & Kleiner, 1990; Groleau *et al.*, 2000; Giguet-Covex *et al.*, 2011). However, it has been shown that the preservation of biogenic calcite in lakes drastically decreases with depth, depending on carbonate particle size (Ramisch *et al.*, 1999). In the case of Lake Iseo, water chemistry indicates the reach of a steady state in $[Ca^{2+}]$ around 100 m (Fig. 5), suggesting that, below this depth, most of the biogenic calcite settling from the surface has been dissolved. One may thus assume that, if lateral sources of event layers exist, they should be located on <30° and <100 m deep slopes overhanging SEB18. Figure 5C and D show the distribution of such areas.

Chemical distinction between sediments coming from the delta and from lateral sources

Distinguishing between those sources basically consists of determining biogenic versus detrital dominant source of carbonate. Given that lacustrine waters are depleted in strontium relative to seawaters (e.g. Brown & Severin, 2009, and references therein; Faure *et al.*, 1967), lacustrine biogenic carbonates generally present a Ca/Sr ratio higher than marine carbonates that partly constitute the lake watershed geological basement (Faure *et al.*, 1967). Hence, the Ca/Sr ratio can be used to distinguish sediment with dominant detrital inputs (lower Ca/Sr value) from sediment more influenced by in-lake biogenic carbonate precipitation (higher Ca/Sr value). As the background sedimentation is composed by no or very few biogenic carbonates, due to carbonate dissolution in the water column (Fig. 5), the mean Ca/Sr value of an event layer (Ca/Sr_{mean}) with a detrital origin is supposed to be equal or lower than the mean Ca/Sr value of the background sedimentation (Ca/Sr_{consed}). On the contrary, event layers with a $Ca/Sr_{mean} > Ca/Sr_{consed}$ are interpreted as relatively enriched in lacustrine biogenic carbonate and thus deriving from lateral sources (Fig. 6A).

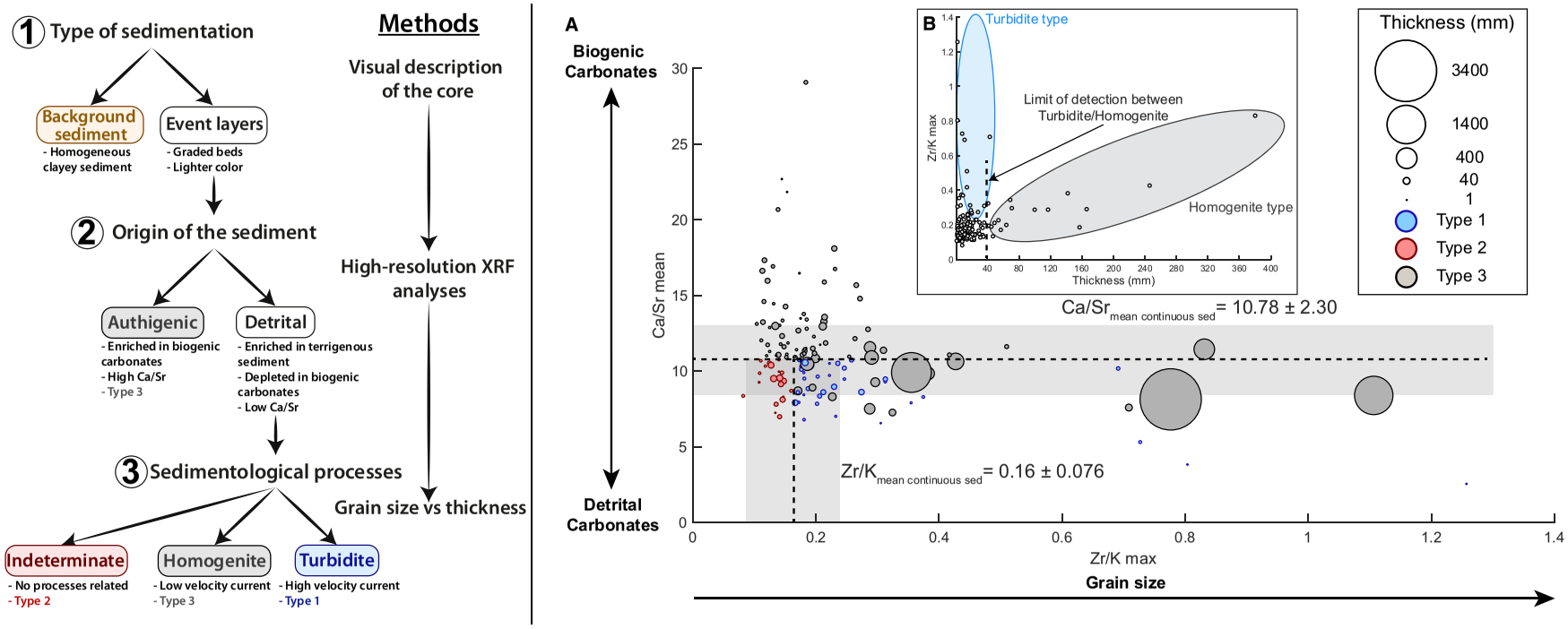

Fig. 6. (A) Scatter plot of Ca/Sr_{mean} versus Zr/K_{max} with the thickness indicate by dot sizes of each event layer. (B) Scatter plot of Zr/K_{max} values versus the thickness of each event layer. Explanation of the methodological approach is synthetized on the left panel.

Distinguishing flood deposits and mass wasting deposits originating from the delta

If lateral can be distinguished from detrital (Oglio delta origin) sediment sources, it remains uncertain whether a detrital event layer was triggered by a flood or by a collapse of the Oglio delta. Due to the distal position of SEB18 relative to the Oglio delta, only massive delta collapse-triggered deposits or extreme flood-triggered underflows, which may run over long distances on the bottom of the lake, may reach the coring site. The relationship between the maximum grain size and the thickness of event layers may here be useful to discriminate the transport processes leading to the deposition of these layers (Fig. 6B, Wilhelm *et al.*, 2013). The MWD are generally more sediment-loaded than flood-triggered underflows (Fanetti *et al.*, 2008; Wilhelm *et al.*, 2013). Consequently, the grain size in MWD is lower than that of underflow deposits due to a more important dilution of coarse particles by the clayey matrix that supports the sediment transport. Hence, it may be assumed here that, for a given grain size, a MWD will be much thicker than a flood-triggered deposit (Wilhelm *et al.*, 2013).

To represent potential variations in grain size within the 146 event layers, the maximum value of Zr/K ratio was used, a chemical proxy of grain size (e.g. Cuven *et al.*, 2011; Wilhelm *et al.*, 2013; Sabatier *et al.*, 2017; Rapuc *et al.*, 2019). Indeed, in lake sediments, Zr is interpreted as a proxy of heavy minerals, while K is linked to fine-grained particles such as clay (Cuven *et al.*, 2010; Kylander *et al.*, 2011). Layers presenting Zr/K_{max} values lower than the mean background sedimentation value were separated from the other detrital layers and their transport processes were not interpreted. A hierarchical clustering on principal components (HCPC) was conducted and allows to distinguish two groups of event layers depending on their thickness and Zr/K_{max} values (Data S2; Fig. 6B). The first cluster presents layers with the highest Zr/K_{max} values (Fig. 6B). These layers are interpreted as composed of coarse grains with a low volume of transported sediment, which requires strong water currents such as turbiditic currents during floods and resulting underflows (Sturm & Matter, 1978). Event layers linked to a MWD are not linked to water flow and thus are supposed to present, on average, a lower grain size for a similar thickness (Fig. 6B; Wilhelm *et al.*, 2013). The authors hence interpret layers from the second cluster as homogenite-type deposits linked to MWD from slopes or deltas.

Attributing triggering mechanism to event layers

The combination of Ca/Sr_{mean} as a proxy of the sediment source, with Zr/K_{max} and the thickness of each event layer as proxies of transport processes, allows to distinguish and interpret the origin among the three different types of layers (Fig. 6). Type 1 regroups thin layers (<40 mm) presenting high Zr/K_{max} and low Ca/Sr_{mean} values (Fig. 6). These layers are interpreted as composed of detrital sediment transported by an underflow. Underflows that reach the deep basin of Lake Iseo can only be linked to extreme flood events from the Oglio river or from the small hillslopes' tributaries. Forty flood layers were hence counted and represent a total thickness of 42 cm. Twenty-one layers, accounting for a thickness of 28 cm present low Zr/K_{max} and low Ca/Sr values, reflecting thin detrital layers or inputs depleted in biogenic carbonates. These layers, labelled as Type 2 layers, are not interpreted because they can be linked either to floods from small tributaries associated with a weak current that does not transport coarse grains or to MWDs from slopes depleted in biogenic carbonates, namely, located in the hypolimnion (below 100 m b.l.s.) where biogenic production is poorly preserved due to low oxygen concentration and pH (Fig. 5). Type 3 regroups: (i) layers presenting high Ca/Sr_{mean} and low Zr/K_{max} values that are composed of sediment enriched in biogenic carbonates coming from smooth slopes above 100 m b.l.s around the core site (Fig. 5D); and (ii) thick layers (>40 mm) composed of detrital materials (low Ca/Sr) that originate from the Oglio delta or smaller tributary deltas. The relationship between the thickness and the Zr/K_{max} of this last group corresponds to a slide or slump-like transport (Fig. 6B). Type 3 layers regroup the three thickest deposits and all layers composed of sediment previously deposited in the lake and remobilized after seismic shaking or sediment overloading. Eighty-five layers linked to such processes were counted and represent 8.81 m of sediment in the SEB18 sequence. Fifteen layers originate from the Oglio delta, and the other 69 layers, enriched in biogenic carbonate, probably originate from lateral slopes. This result suggests that Lake Iseo sediment

accumulation is a good candidate to have recorded seismic activity.

To strengthen the interpretation of event layer triggering mechanisms, the ages of several events with the Italian historical seismic catalogue (CPTI15, Rovida *et al.*, 2019, 2020) and local documented flood events (Luino *et al.*, 2002; Guzzetti & Tonelli, 2004) were compared. The three thickest Type 3 layers (EL1, EL2 and EL3) originate from the Oglio delta which is several kilometres long and is the principal source that can produce 1.3 to 3.4 m thick detrital layers. Altogether, those three events moved a total of *ca* 100 km^3 to the lake basin. EL1 (11 km^3), is dated between 1120 CE and 1220 CE; considering ^{14}C dating uncertainties, it can be correlated to the 1222 CE earthquake that caused heavy damage in the Brescia area (<30 km distance from the lake). Despite the fact that the earthquake source cannot be precisely identified from both geological surveys (e.g. Livio *et al.*, 2009) and macroseismic data (Guidoboni *et al.*, 2005); the earthquake parameters are largely imprecise (see a comparison of epicentral location, and derived magnitude at https://emidius.mi.ingv.it/ASMI/event/12221225_1230_000), the historical chronicle refers to repeated events, and damages that are compatible with low frequency, long duration shakings. This seismic event had moreover been identified yet in another Lake Iseo sub-basin (SEB05 and SEB06 sequences; Lauterbach *et al.*, 2012) and in Lake Como (Fig. 1, Fanetti *et al.*, 2008) where it has been associated with a *ca* 3 km^3 megaturbidite deposit. The thickest Type 3 layer, EL2, is dated between 1020 CE and 1125 CE and can be attributed to the 1117 CE earthquake: this event is one of the strongest and most damaging historical earthquakes documented in northern Italy (Galadini *et al.*, 2001; Gasperini *et al.*, 2004). It occurred probably south of Verona (about 80 km distance, south-eastward of Lake Iseo) with damage of intensity VII MCS both in Brescia and Milan; the expected shakings in the lake area should have been therefore similar to the one caused by the 1222 earthquake. Alternatively, this layer could be attributed to the 1065 CE Brescia earthquake, for which only two macroseismic observations (Brescia, VIII; Milan, Felt) are available, and the level of ground motion at Lake Iseo is highly speculative. The background sedimentation intercalated between these two thick event layers represents around 93 years, which, considering that the base of EL2 is erosive, almost corresponds to the time gap between the two historical seismic events. The oldest thick Type 3 layer, EL3, is dated between 640 CE and 830 CE. For this event there is no earthquake in the Italian historical macroseismic archive (https://emidius.mi.ingv.it/ASMI/) that could reasonably be associated with the layer, but it is known that in the Middle Ages the database is incomplete, also for major events. The nearest earthquake in time and space is the one referred to Treviso in 778 CE, but the expected ground motion at Lake Iseo due to this earthquake cannot be responsible for massive slope instabilities. Another megaturbidite that led to a *ca* 10.5 km^3 sediment deposit resulting from large MWD from steep slopes was recorded in Lake Como (Fanetti *et al.*, 2008) and might coincide with another megaturbidite deposit in Lake Sils dated at *ca* 700 CE (Blass *et al.*, 2005).

To go further, few to no major mass wasting deposits are visible underneath the coring area on the seismic profiles (Fig. 1C and D). The sedimentation rate is supposed to be lower regionally before 0 CE (Ravazzi *et al.*, 2013; Vannière *et al.*, 2013; Arnaud *et al.*, 2016; Rapuc *et al.*, 2019). Thus, during periods of low sedimentation rate, very few to no mass wasting deposits occurred, making the hypothesis of an autogenic origin for all the mass wasting deposits very unlikely.

Concerning Type 1 layers, some of the most recent layers present the same ages as local and regional historical flood events such as the 1991, 1960 and 1952 floods that impacted the city of Darfo Boario Terme (Luino *et al.*, 2002) or the 1994 regional flood event that impacted the Po Plain (Guzzetti & Tonelli, 2004).

Link between sediment inputs and the frequency of sediment remobilization

A sediment yield (SY; t km^{-2} $year^{-1}$) was calculated to characterize the evolution of erosion rates in the anthropized area of Lake Iseo watershed, i.e. the low to mid-altitude part of the catchment (Rapuc *et al.*, 2021a), and was interpreted as mainly influenced by human activities. This erosion signal presents a two-fold increase between the early Common Era and 750 CE (Fig. 7A). Two other periods of enhanced erosion in the watershed have been registered between 950 CE and 1350 CE and from 1650 CE to the present. The frequency of Type 1 and Type 3 layers, interpreted as linked to flood and earthquakes events, respectively, are presented as variation of the number of events per 101 years (Fig. 7B). Interpretation of

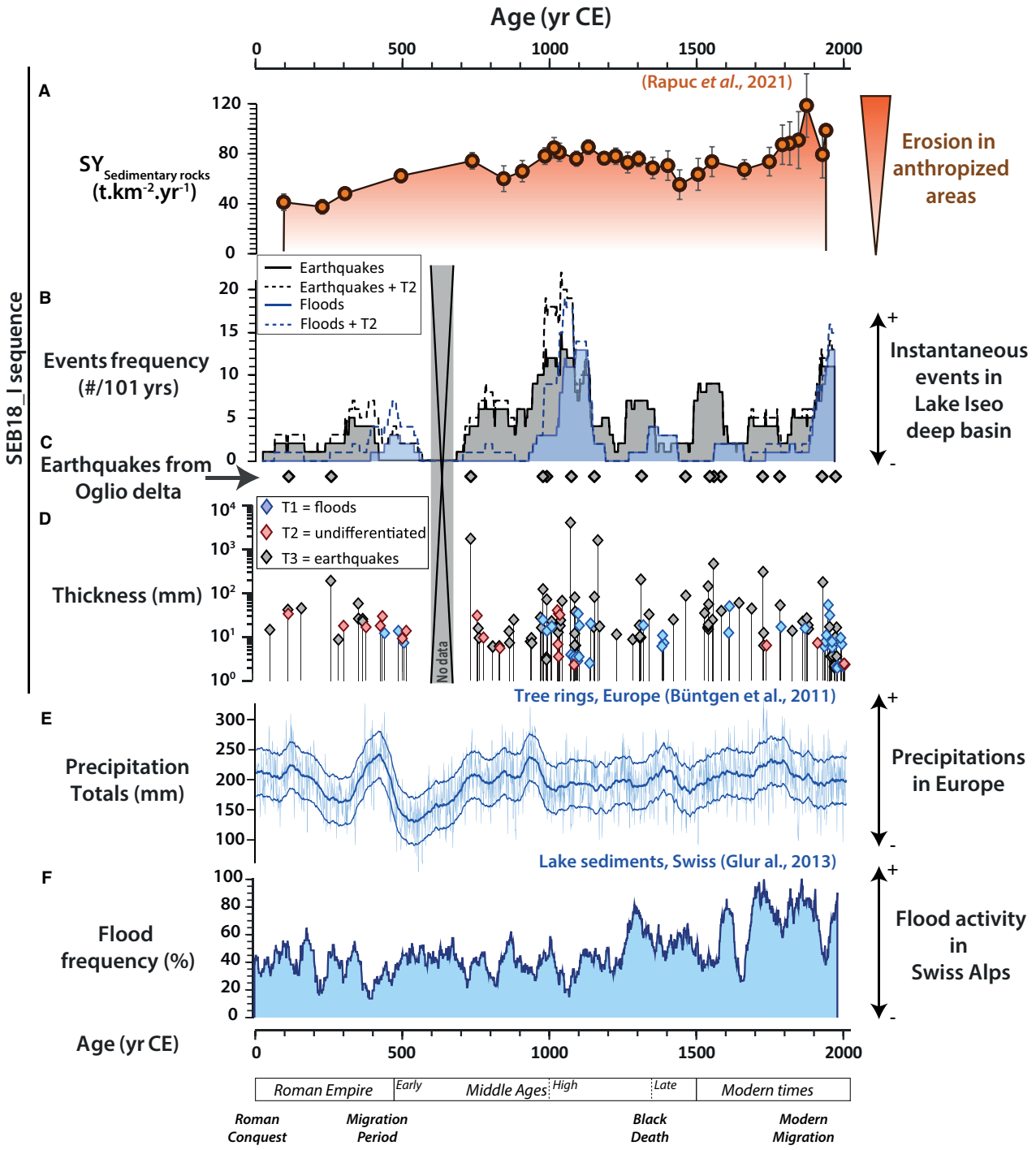

Fig. 7. Comparison of the main results obtained on SEB18 sediment sequence with regional climatic information plotted against the age. (A) The sediment yield of the anthropized area of the Iseo watershed (in t km^{-2} $year^{-1}$) obtained from Rapuc *et al.* (2021). The erosion of this area was interpreted as being mainly influenced by human activities. (B) SEB18 flood and earthquake frequency obtained from ages of Type 1 and Type 3 layers, respectively, Type 1 and 2, and Type 3 and 2 sums are plotted in dotted lines. (C) Type 3 layers with a detrital composition. (D) Thickness of each kind of layer. (E) Reconstructed AMJ precipitation totals modified from Büntgen *et al.* (2011). (F) 50-year moving average of flood events from Swiss lakes, modified from Glur *et al.* (2013).

fluctuations of these frequencies between 580 CE and 670 CE should be taken with caution due to a gap in the sediment section.

Flood and sediment availability

The flood frequency recorded during the Roman Period differs from the local and regional trends: several studies attested evidence of increase flood occurrences at that time (e.g. Glur *et al.*, 2013; Vannière *et al.*, 2013; Wirth *et al.*, 2013b; Rossato *et al.*, 2015) but no increase is detected in the Lake Iseo deep basin until approximately 950 CE. This increase led to high frequency between 950 CE and 1150 CE which are in good agreement with periods of high flood frequencies recorded in river sediments of north-eastern Italy (Rossato *et al.*, 2015) and in Lake Ledro (Vannière *et al.*, 2013; Wirth *et al.*, 2013a). Yet, these high frequencies are disconnected from the trend observed in the Swiss Alps (Fig. 7; Glur *et al.*, 2013). There is also no increase recorded in the Iseo deep basin during the Little Ice Age (LIA) when all of the local and regional studies record an important flood activity due to a colder and wetter climate (Glur *et al.*, 2013; Vannière *et al.*, 2013; Wirth *et al.*, 2013a,b). During the last century, a sharp increase is recorded, starting at *ca* 1890 CE (Fig. 7), which seems to be in agreement with the observed frequency in the Swiss Alps (Fig. 7; Glur *et al.*, 2013) but differs from the regional trend (Wirth *et al.*, 2013a,b).

Thus, it appears that the flood frequency recorded in the deep basin of Lake Iseo does not directly follow regional climate fluctuations and is decorrelated from regional flood activities. The comparison between the average values per 100 years between the SEB18 flood frequency and the regional flood activities from Glur *et al.* (2013) shows a clear decorrelation ($r = 0.1$; *P-value* $<1.6 \times 10^{-10}$) throughout the last 2000 years. Periods of high flood frequency occur during times of high erosion rates in the low to mid altitude areas of the Iseo watershed, as shown by the good correlation between the average values per 100 years of the two curves (Fig. 7A and B; $r = 0.6$; *P*-value $<2.3 \times 10^{-13}$). These periods, are thus characterized by high sediment accumulation in the watershed, increasing the sediment available to be remobilized by a precipitation event in the watershed. The highest flood frequency recorded occurred together with the occurrence of the two biggest historical earthquakes that impacted the Val Camonica (i.e. 1117 CE and 1222 CE). Those earthquakes might have also favoured sediment availability in the watershed, leading to an increase of sediment remobilization by precipitation and thus to an increase of the number of turbidites recorded in Iseo lake sediments. Such a phenomenon has already been reported elsewhere, for instance in the New-Zealand Southern Alps (Howarth *et al.*, 2012; Wang *et al.*, 2020).

Earthquakes and sediment availability

The earthquake frequency recorded in Lake Iseo deep basin starts to increase at 750 CE to reach high values (12 per 101 years) between 950 CE and 1150 CE. High frequencies are also recorded during 1250 to 1350, 1500 to 1600 CE periods and from 1850 CE to the present. This study observed that the frequency of recorded earthquakes is high during or just after a long period of sediment accumulation in the lake, i.e. a period of high erosion rate in the watershed (Fig. 7A). The comparison between the average values per 100 years of the SEB18 earthquake frequency and the erosion signal from the Iseo watershed indicates a strong correlation ($r = 0.6$; *P*-value $<2.6 \times 10^{-13}$). It was also observed that the earthquake frequency decreases sharply after the remobilization of a large volume of sediment from slopes or the delta (Fig. 7C). Indeed, after the occurrence of the three thickest layers, linked to *ca* 778 CE, 1117 CE and 1222 CE earthquake events, no deposits from the Oglio delta are recorded for a long period, leading to an apparent decrease in the earthquake frequency.

Moreover, from the seismic profiles (Fig. 1C and D) and previous seismic survey conducted on Lake Iseo deep basin (Bini *et al.*, 2007), no important MWDs seem to occur underneath the bottom of the SEB18 sediment sequence (21 CE). In the sediment succession of Sale Marasino Basin, the only thick deposits linked to seismic activity occurred within the last 2500 years (Lauterbach *et al.*, 2012). A possible explanation could be the progressive increase of erosion in the watershed from the Neolithic, reaching high levels during the Roman Period, as attested to by previous works in Lake Iseo (Lauterbach *et al.*, 2012; Rapuc *et al.*, 2019) and regionally (e.g. Giguet-Covex *et al.*, 2011; Vannière *et al.*, 2013; Joannin *et al.*, 2014; Andrič *et al.*, 2020). Indeed, when long-term erosion increases, the accumulation of sediment on lake slopes and delta increases, leading to high sediment availability to earthquake induced remobilization. Increasing in turn the sensitivity of the lake to record

earthquakes (Wilhelm *et al.*, 2016; Rapuc *et al.*, 2018; Gastineau *et al.*, 2021).

It has been established on faults in Central Italy, especially in the Apennines, that periods of high seismic activities last several hundred years and are separated by long quiescence periods (e.g. Benedetti *et al.*, 2013; Verdecchia *et al.*, 2018). The link between high earthquake frequency periods registered in Lake Iseo and sediment availability is then reinforced by the absence of short-term seismic variability evidence in the Italian regions that could have been at the origin of the here recorded frequency evolution.

Linking human-influence and sediment supply

At the beginning of the Roman Period, the erosion in the Lake Iseo watershed is high (Rapuc *et al.*, 2021a) compared to what has been measured in other peri-Alpine lakes (Arnaud & Révillon, 2015), suggesting that erosion in the Val Camonica was already important before the Roman Period and increases until 750 CE. (Fig. 7). From the Iron Age, a high number of rock carvings and several Camuni cities are identified in the southern part of the watershed, indicating that the Camuni society was well-developed (Anati & Cittadini, 1994; Anati, 2009; Casini & De Marinis, 2009). Several palynological records indicate that agricultural activities first start around 4 kyr BP in the Val Camonica, associated with human-induced deforestation and fire activity in the southern Alps (Gobet *et al.*, 2000; Comiti, 2012; Iglesias *et al.*, 2019) and mid-altitude pastoralism from 3 kyr BP (Pini, 2002; Pini *et al.*, 2016). All of this evidence, associated with previous studies on lake sediment in the southern and Julian Alps (Joannin *et al.*, 2014; Rapuc *et al.*, 2018, 2019, 2021a; Andrič *et al.*, 2020), suggests that human activities had already impacted the erosion and sediment transport processes in the main watersheds of the southern Alps before the Roman Period.

From that Period towards the present, this study has demonstrated that the erosion from the low to mid altitude areas of the Lake Iseo watershed was predominantly linked to human activities. This previous work was conducted on the same sediment sequence, i.e. SEB18, using isotopic geochemistry and a source-to-sink approach (Rapuc *et al.*, 2021a). The development of agricultural and pastoral practices, linked to a general increase of the human population in the area inducing a modification of the vegetation cover, were interpreted as the main drivers of a three-fold increase in erosion rates in the Lake Iseo watershed throughout the last 2000 years (Fig. 7A).

Human influence on erosion and transport processes

The comparison between the sedimentary processes that occurred in Lake Iseo deep basin and the knowledge of geodynamic, climate and human activities throughout the last 2000 years in the Italian southern Alps helped to understand the drivers of the local erosion (Rapuc *et al.*, 2021a). It appears that, from the Roman Period, human activities by increasing agricultural activities, grazing and deforestations have induced a general increase in sediment input towards depositional sinks (Fig. 7A; Rapuc *et al.*, 2021). After a delay due to transport processes and sediment storage in the watershed, the increased amount of sediment brought to intermediate sinks is stocked on lake deltas and slopes. This abnormal sediment accumulation led to an increase of the sedimentation rate in the deep basin and, after periods of high sediment input, caused an increase of destabilization of slopes or delta due to seismic shaking or sediment overloading (Fig. 8; Wilhelm *et al.*, 2016; Rapuc *et al.*, 2018; Gastineau *et al.*, 2021). Equally, due to increased sediment availability in lake catchment, the sediment load during a flood event increased, leading to an increase of flood frequency recorded in lake sediments independent of climate fluctuations (Fig. 8), as previously observed in other lake systems (e.g. Giguet-Covex *et al.*, 2012; Howarth *et al.*, 2012; Brisset *et al.*, 2017). Then, even in large lake catchments, human activities through deforestation, pastoralism and agriculture, affect the erosion processes and the resulting sediment transport and remobilization. The increase of sediment availability by human activity causes a disconnection between the recorded instantaneous event frequency from the occurrence of their geodynamic or climatic triggers, and thus impacts the sensitivity of a lake as a natural archive to record the earth-surface processes. Thus, in the case where the storage of sediment in the watershed and on the slopes and the delta varies through time, the considered lake system will not directly record an answer from an external forcing such as a precipitation event or earthquake shaking but will be dependent on

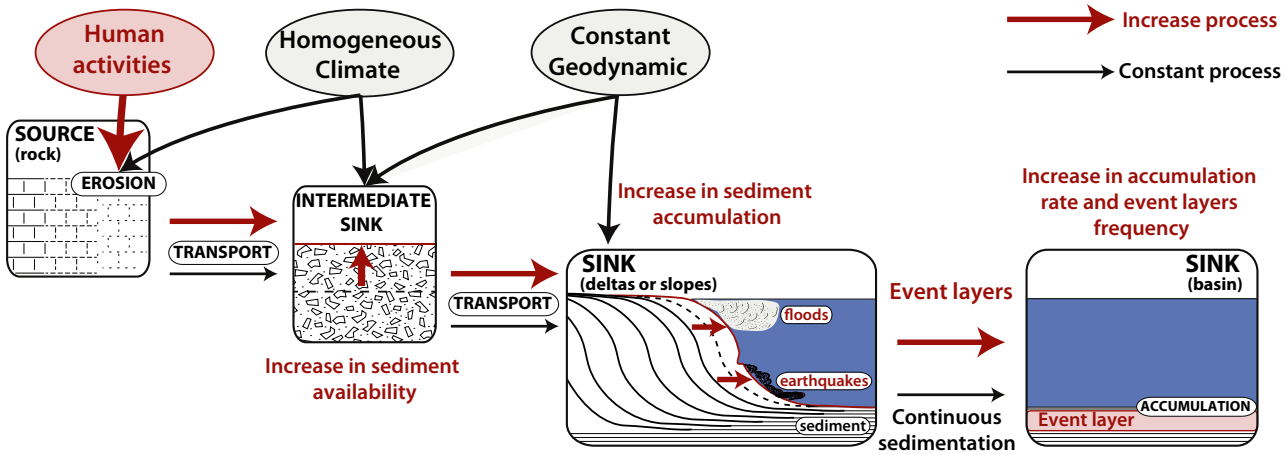

Fig. 8. Conceptual model of the erosion cycle in a large catchment and the effects of the three main forcing factors (human activities, climate and geodynamic). Modified from Rapuc *et al.* (2021b).

the sediment availability as expressed on Fig. 8. This is especially the case in large lowland lake systems such as peri-Alpine lakes that are located at the end of an important watershed where climate and human activities interplay for several thousand years on erosion processes.

CONCLUSION

In a large and deep lake, like Iseo, the sediment may originate from several different sources which makes difficult to disentangle the processes that triggered the deposit of event layers. The use of X-ray fluorescence (XRF) ratios; namely Ca/Sr ratio as a proxy of in-lake sediment sources, and Zr/K ratio associated with the thickness of each layer as proxies of transport processes allowed the authors to attribute most of them to flood or mass wasting events. Considering the evolution of the terrigenous input, this study showed that the apparent frequency of earthquakes recorded in Lake Iseo deep basin is influenced by the sediment available to be remobilized, which in turn depends on the erosion rate within the catchment area. Human practices and, to a lesser extent, climate fluctuations have impacted the available sediment within both the lake slopes and the catchment areas, and thus the recording of extreme geodynamic and climatic events. Even in large catchment areas, human activities can play a key role on erosion processes and sediment availability which may affect the recording of the earth-surface processes. Hence, discussing instant events frequency recorded in sediments from deep lakes should only be done after a thorough study of the human activity in the watershed. Moreover, the question of sediment availability in a lake system and its watershed should always be predominant in the instant events frequency studies.

ACKNOWLEDGEMENTS

This work was conducted in the framework of the CRITLAKE project funded by the AAP Université Savoie Mont Blanc in 2018 and thanks to the support of the entire staff of the C2FN-DT-INSU associated to the CLIMCORE project. Thanks to Qi Lin for his support and great help on the coring survey. Thanks to the Associazione Nazionale dei Carabinieri (Cesare Miniaci, Michele Liso and colleagues) for assistance on the lake, the use of their boat for the seismic survey and the anchoring of the platform. ^{14}C analyses were acquired thanks to the CNRS-INSU ARTEMIS national radiocarbon AMS measurement programme at Laboratoire de Mesure 14C (LMC14) in the CEA Institute at Saclay (French Atomic Energy Commission). The authors would also like to thank the Laboratoire Souterrain de Modane facilities for the gamma spectrometry measurements. Thanks to Kim Genuite for valuable help with GIS processing and the creation of the maps. Thanks to Lucilla Benedetti, Roberta Pini, Giulia Valerio and Marco Pilotti for their helpful advice. Thanks to Christian Crouzet for his help in the

understanding of transport processes at the origin of the main layers. Finally we want to thank the Associate Editor Kyle Straub and an anonymous reviewer for their helpful comments.

DATA AVAILABILITY STATEMENT

The data that support the findings of this study are available from the corresponding author upon reasonable request.

REFERENCES

Adams, E.W., **Schlager, W.** and **Anselmetti, F.S.** (2001) Morphology and curvature of delta slopes in Swiss lakes: lessons for the interpretation of clinoforms in seismic data. *Sedimentology*, **48**, 661–679.

Ambrosetti, W. and **Barbanti, L.** (2005) Evolution towards meromixis of Lake Iseo (Northern Italy) as revealed by its stability trend. *J. Limnol.*, **64**, 1.

Anati, E. (2009) L'art rupestre du Valcamonica : évolution et signification. Une vision panoramique d'après l'état actuel de la recherche. *L'anthropologie*, **113**, 930–968.

Anati, E. and **Cittadini, T.** (1994) *Valcamonica Rock Art: A New History for Europe*. Edizioni del Centro, Capo di Ponte.

Andrič, M., **Sabatier, P.**, **Rapuc, W.**, **Ogrinc, N.**, **Dolenec, M.**, **Arnaud, F.**, **von Grafenstein, U.** and **Šmuc, A.** (2020) 6600 years of human and climate impacts on lake-catchment and vegetation in the Julian Alps (Lake Bohinj, Slovenia). *Quat. Sci. Rev.*, **227**, 106043.

Appleby, P.G., **Richardson, N.** and **Nolan, P.J.** (1991) 241Am dating of lake sediments. In: *Environmental History and Palaeolimnology* (Eds Smith, J.P., Appleby, P.G., Battarbee, R.W., Dearing, J.A., Flower, R., Haworth, E.Y., Oldfield, F. and O'Sullivan, P.E.), pp. 35–42. Springer Netherlands, Dordrecht.

Arnaud, F. (2005) Discriminating bio-induced and detrital sedimentary processes from particle size distribution of carbonates and non-carbonates in hard water lake sediments. *J. Paleolimnol.*, **34**, 519–526.

Arnaud, F., **Lignier, V.**, **Revel, M.**, **Desmet, M.**, **Beck, C.**, **Pourchet, M.**, **Charlet, F.**, **Trentesaux, A.** and **Tribovillard, N.** (2002) Flood and earthquake disturbance of 210Pb geochronology (Lake Anterne, NW Alps). *Terra Nova*, **14**, 225–232.

Arnaud, F., **Poulenard, J.**, **Giguet-Covex, C.**, **Wilhelm, B.**, **Révillon S.**, **Jenny, J.-P.**, **Revel, M.**, **Enters, D.**, **Bajard, M.**, **Fouinat, L.**, **Doyen, E.**, **Simonneau, A.**, **Pignol, C**, **Chapron, E.**, **Vannière, B.** and **Sabatier, P.** (2016) Erosion under climate and human pressures: An alpine lake sediment perspective. *Quat. Sci. Rev.*, **152**, 1–18. http://doi.org/10.1016/j.quascirev.2016.09.018

Arnaud, F. and **Révillon, S.** (2015) A geochemical approach to improve radiocarbon-based age-depth models in non-laminated sediment series. In: *Micro-XRF Studies of Sediment Cores: Applications of a Non-Destructive Tool for the Environmental Sciences* (Eds Croudace, I.W. and Rothwell, R.G.), pp. 459–472. Springer Netherlands, Dordrecht.

Bajard, M., **Sabatier, P.**, **David, F.**, **Develle, A.-L.**, **Reyss, J.-L.**, **Fanget, B.**, **Malet, E.**, **Arnaud, D.**, **Augustin, L.**, **Crouzet, C.**, **Poulenard, J.** and **Arnaud, F.** (2016) Erosion record in Lake La Thuile sediments (Prealps, France): evidence of montane landscape dynamics throughout the Holocene. *Holocene*, **26**, 350–364.

Benedetti, L., **Manighetti, I.**, **Gaudemer, Y.**, **Finkel, R.**, **Malavieille, J.**, **Pou, K.**, **Arnold, M.**, **Aumaître, G.**, **Bourlès, D.** and **Keddadouche, K.** (2013) Earthquake synchrony and clustering on Fucino faults (Central Italy) as revealed from in situ 36Cl exposure dating. *J. Geophys. Res. Solid Earth*, **118**, 4948–4974.

Bini, A., **Cita, M.B.** and **Gaetani, M.** (1978) Southern Alpine Lakes—Hypothesis of an erosional origin related to the Messinian entrenchment. *Mar. Geol.*, **27**, 271–288.

Bini, A., **Corbari, D.**, **Falletti, P.**, **Fassina, M.**, **Perotti, C.R.** and **Piccin, A.** (2007) Morphology and geological setting of Iseo Lake (Lombardy) through multibeam bathymetry and high-resolution seismic profiles. *Swiss J. Geosci.*, **100**, 23–40.

Blaauw, M. (2010) Methods and code for 'classical'age-modelling of radiocarbon sequences. *Quat. Geochronol.*, **5**, 512–518.

Blass, A., **Anselmetti, F.S.**, **Grosjean, M.** and **Sturm, M.** (2005) The last 1300 years of environmental history recorded in the sediments of Lake Sils (Engadine, Switzerland). *Swiss J. Geosci.*, **98**, 319–332.

Brisset, E., **Guiter, F.**, **Miramont, C.**, **Troussier, T.**, **Sabatier, P.**, **Poher, Y.**, **Cartier, R.**, **Arnaud, F.**, **Malet, E.** and **Anthony, E.J.** (2017) The overlooked human influence in historic and prehistoric floods in the European Alps. *Geology*, **45**, 347–350.

Brown, R.J. and **Severin, K.P.** (2009) Otolith chemistry analyses indicate that water Sr: Ca is the primary factor influencing otolith Sr: Ca for freshwater and diadromous fish but not for marine fish. *Can. J. Fish. Aquat. Sci.*, **66**, 1790–1808.

Bruel, R., **Marchetto, A.**, **Bernard, A.**, **Lami, A.**, **Sabatier, P.**, **Frossard, V.** and **Perga, M.-E.** (2018) Seeking alternative stable states in a deep lake. *Freshw. Biol.*, **63**, 553–568.

Bruel, R. and **Sabatier, P.** (2020) serac: an R package for ShortlivEd RAdionuclide chronology of recent sediment cores. *J. Environ. Radioact.*, **225**, 106449.

Büntgen, U., **Myglan, V.S.**, **Ljungqvist, F.C.**, **McCormick, M.**, **Di Cosmo, N.**, **Sigl, M.**, **Jungclaus, J.**, **Wagner, S.**, **Krusic, P.J.**, **Esper, J.**, **Kaplan, J.O.**, **de Vaan, M.A.C.**, **Luterbacher, J.**, **Wacker, L.**, **Tegel, W.** and **Kirdyanov, A.V.** (2016) Cooling and societal change during the Late Antique Little Ice Age from 536 to around 660 AD. *Nat. Geosci.*, **9**, 231–236.

Büntgen, U., **Tegel, W.**, **Nicolussi, K.**, **McCormick, M.**, **Frank, D.**, **Trouet, V.**, **Kaplan, J.O.**, **Herzig, F.**, **Heussner, K.-U.**, **Wanner, H.**, **Luterbacher, J.** and **Esper, J.** (2011) 2500 years of European climate variability and human susceptibility. *Science*, **331**, 578–582.

Casini, S. and **De Marinis, R.** (2009) Des pierres et des dieux. L'art rupestre de la Valteline et du Valcamonica. *Globe Rev. Genevoise Géographie*, **149**, 61–92.

Chapron, E., **Simonneau, A.**, **Ledoux, G.**, **Arnaud, F.**, **Lajeunesse, P.** and **Albéric, P.** (2016) French alpine foreland holocene paleoseismicity revealed by coeval mass wasting deposits in glacial lakes. In: *Submarine Mass Movements and their Consequences*, pp. 341–349. Springer, Cham.

Comiti, F. (2012) How natural are Alpine mountain rivers? Evidence from the Italian Alps. *Earth Surf. Process. Landf.*, **37**, 693–707.

Cuven, S., **Francus, P.** and **Lamoureux, S.F.** (2010) Estimation of grain size variability with micro X-ray fluorescence in laminated lacustrine sediments, Cape Bounty, Canadian High Arctic. *J. Paleolimnol.*, **44**, 803–817.

Cuven, S., **Francus, P.** and **Lamoureux, S.** (2011) Mid to Late Holocene hydroclimatic and geochemical records from the varved sediments of East Lake, Cape Bounty, Canadian High Arctic. *Quat. Sci. Rev.*, **30**, 2651–2665.

Dal Piaz, G.V., **Bistacchi, A.** and **Massironi, M.** (2003) Geological outline of the Alps. *Episodes*, **26**, 175–180.

DISS Working Group (2018) Database of Individual Seismogenic Sources (DISS), version 3.2.1. 127 Individual Seismogenic Sources, 188 Composite Seismogenic Sources, 35 Debated Seismogenic Sources, 3 Subduction Zones.

Dotterweich, M., **Stankoviansky, M.**, **Minár, J.**, **Koco, Š.** and **Papčo, P.** (2013) Human induced soil erosion and gully system development in the Late Holocene and future perspectives on landscape evolution: the Myjava Hill Land, Slovakia. *Geomorphology*, **201**, 227–245.

Doyen, É., **Vannière, B.**, **Berger, J.-F.**, **Arnaud, F.**, **Tachikawa, K.** and **Bard, E.** (2013) Land-use changes and environmental dynamics in the upper Rhone valley since Neolithic times inferred from sediments in Lac Moras. *Holocene*, **23**, 961–973.

Edwards, K.J. and **Whittington, G.** (2001) Lake sediments, erosion and landscape change during the Holocene in Britain and Ireland. *Catena*, **42**, 143–173.

Fanetti, D., **Anselmetti, F.S.**, **Chapron, E.**, **Sturm, M.** and **Vezzoli, L.** (2008) Megaturbidite deposits in the Holocene basin fill of Lake Como (southern Alps, Italy). *Palaeogeogr. Palaeoclimatol. Palaeoecol.*, **259**, 323–340.

Faure, G., **Crocket, J.H.** and **Hueley, P.M.** (1967) Some aspects of the geochemistry of strontium and calcium in the Hudson Bay and the Great Lakes. *Geochim. Cosmochim. Acta*, **31**, 451–461.

Fouinat, L., **Sabatier, P.**, **Poulenard, J.**, **Etienne, D.**, **Crouzet, C.**, **Develle, A.-L.**, **Doyen, E.**, **Malet, E.**, **Reyss, J.-L.**, **Sagot, C.**, **Bonet, R.** and **Arnaud, F.** (2017) One thousand seven hundred years of interaction between glacial activity and flood frequency in proglacial Lake Muzelle (western French Alps). *Quat. Res.*, **87**, 407–422.

Fouinat, L., **Sabatier, P.**, **David, F.**, **Montet, X.**, **Schoeneich, P.**, **Chaumillon, E.**, **Poulenard, J.** and **Arnaud, F.** (2018) Wet avalanches: long-term evolution in the Western Alps under climate and human forcing. *Clim. past*, **14**, 1299–1313.

Francke, A., **Dosseto, A.**, **Panagiotopoulos, K.**, **Leicher, N.**, **Lacey, J.H.**, **Kyrikou, S.**, **Wagner, B.**, **Zanchetta, G.**, **Kouli, K.** and **Leng, M.J.** (2019) Sediment residence time reveals Holocene shift from climatic to vegetation control on catchment erosion in the Balkans. *Glob. Planet. Change*, **177**, 186–200.

Fuchs, M. (2007) An assessment of human versus climatic impacts on Holocene soil erosion in NE Peloponnese. *Greece. Quat. Res.*, **67**, 349–356.

Galadini, F., **Galli, P.**, **Molin, D.** and **Ciurletti, G.** (2001) Searching for the source of the 1117 earthquake in northern Italy: a multidisciplinary approach. In: *The Use of Historical Data in Natural Hazard Assessments*, pp. 3–27. Springer, Dordrecht.

Garibaldi, L., **Anzani, A.**, **Marieni, A.**, **Leoni, B.** and **Mosello, R.** (2003) Studies on the phytoplankton of the deep subalpine Lake Iseo. *J. Limnol.*, **62**, 177–189.

Garibaldi, L., **Mezzanotte, V.**, **Brizzio, M.**, **Rogora, M.** and **Mosello, R.** (1999) The trophic evolution of Lake Iseo as related to its holomixis. *J. Limnol.*, **58**, 10–19.

Gasperini, P., **Camassi, R.**, **Mirto, C.** and **Stucchi, M.** (2004) *Catalogo Parametrico dei Terremoti Italiani, versione CPTI04*. Istituto Nazionale di Geofisica e Vulcanologia (INGV), Bologna.

Gastineau, R., **de Sigoyer, J.**, **Sabatier, P.**, **Fabbri, S.C.**, **Anselmetti, F.S.**, **Develle, A.L.**, **Şahin, M.**, **Gündüz, S.**, **Niessen, F.** and **Gebhardt, A.C.** (2021) Active subaquatic fault segments in lake Iznik Along the middle strand of the North Anatolian Fault, NW Turkey. *Tectonics*, **40**, e2020TC006404.

Gehrig, R. (1997) *Pollenanalytische Untersuchungen zur Vegetations-und-Klimageschichte des Val Camonica (Norditalien)*. Dissertationes Botanicae 276. J. Cramer, Berlin Stuttgart.

Giardini, D., **Woessner, J.**, **Danciu, L.**, **Crowley, H.**, **Cotton, F.**, **Grünthal, G.**, **Pinho, R.**, **Valensise, G.**, **Akkar, S.** & **Arvidsson, R.** (2013) *Seismic hazard harmonization in Europe (SHARE): online data resource*. https://doi.org/10.12686/SED-00000001-SHARE

Giguet-Covex, C., **Arnaud, F.**, **Poulenard, J.**, **Disnar, J.-R.**, **Delhon, C.**, **Francus, P.**, **David, F.**, **Enters, D.**, **Rey, P.-J.** and **Delannoy, J.-J.** (2011) Changes in erosion patterns during the Holocene in a currently treeless subalpine catchment inferred from lake sediment geochemistry (Lake Anterne, 2063 m asl, NW French Alps): the role of climate and human activities. *Holocene*, **21**, 651–665.

Giguet-Covex, C., **Arnaud, F.**, **Enters, D.**, **Poulenard, J.**, **Millet, L.**, **Francus, P.**, **David, F.**, **Rey, P.-J.**, **Wilhelm, B.** and **Delannoy, J.-J.** (2012) Frequency and intensity of high-altitude floods over the last 3.5 ka in northwestern French Alps (Lake Anterne). *Quat. Res.*, **77**, 12–22.

Giosan, L., **Ponton, C.**, **Usman, M.**, **Blusztajn, J.**, **Fuller, D.Q.**, **Galy, V.**, **Haghipour, N.**, **Johnson, J.E.**, **McIntyre, C.**, **Wacker, L.** and **Eglinton, T.I.** (2017) Short communication: massive erosion in monsoonal central India linked to late Holocene land cover degradation. *Earth Surf. Dyn.*, **5**, 781–789.

Glover, T.J. (1997) *Pocket Ref*, 2nd edn. Sequoia, Littleton, CO, 542 pp.

Glur, L., **Wirth, S.B.**, **Büntgen, U.**, **Gilli, A.**, **Haug, G.H.**, **Schär, C.**, **Beer, J.** and **Anselmetti, F.S.** (2013) Frequent floods in the European Alps coincide with cooler periods of the past 2500 years. *Sci. Rep.*, **3**, 2770.

Gobet, E., **Tinner, W.**, **Hubschmid, P.**, **Jansen, I.**, **Wehrli, M.**, **Ammann, B.** and **Wick, L.** (2000) Influence of human impact and bedrock differences on the vegetational history of the Insubrian Southern Alps. *Veg. Hist. Archaeobot.*, **9**, 175–187.

Groleau, A., **Sarazin, G.**, **Vinçon-Leite, B.**, **Tassin, B.** and **Quiblier-Llobéras, C.** (2000) Tracing calcite precipitation with specific conductance in a hard water alpine lake (Lake Bourget). *Water Res.*, **34**, 4151–4160.

Groppelli, B., **Soncini, A.**, **Bocchiola, D.** and **Rosso, R.** (2011) Evaluation of future hydrological cycle under climate change scenarios in a mesoscale Alpine watershed of Italy. *Nat. Hazards Earth Syst. Sci.*, **11**, 1769–1785.

Guidoboni, E., **Comastri, A.** and **Boschi, E.** (2005) The "exceptional" earthquake of 3 January 1117 in the Verona area (northern Italy): A critical time review and detection of two lost earthquakes (lower Germany and Tuscany). *J. Geophys. Res.*, **110**, 1–20. http://doi.org/10.1029/2005jb003683

Guzzetti, F. and **Tonelli, G.** (2004) Information system on hydrological and geomorphological catastrophes in Italy (SICI): a tool for managing landslide and flood hazards. *Nat. Hazards Earth Syst. Sci.*, **4**, 213–232.

Heiri, O., **Lotter, A.F.** and **Lemcke, G.** (2001) Loss on ignition as a method for estimating organic and carbonate content in sediments: reproducibility and comparability of results. *J. Paleolimnol.*, **25**, 101–110.

Hieke, W. (1984) A thick Holocene homogenite from the Ionian Abyssal Plain (eastern Mediterranean). *Mar. Geol.*, **55**, 63–78.

Hogg, C.A., **Marti, C.L.**, **Huppert, H.E.** and **Imberger, J.** (2013) Mixing of an interflow into the ambient water of Lake Iseo. *Limnol. Oceanogr.*, **58**, 579–592.

Howarth, J.D., **Fitzsimons, S.J.**, **Norris, R.J.** and **Jacobsen, G.E.** (2012) Lake sediments record cycles of sediment flux driven by large earthquakes on the Alpine fault, New Zealand. *Geology*, **40**, 1091–1094.

Iglesias, V., **Vannière, B.** and **Jouffroy-Bapicot, I.** (2019) Emergence and evolution of anthropogenic landscapes in the western Mediterranean and adjacent Atlantic regions. *Fire*, **2**, 53.

Joannin, S., **Magny, M.**, **Peyron, O.**, **Vannière, B.** and **Galop, D.** (2014) Climate and land-use change during the late Holocene at Lake Ledro (southern Alps, Italy). *Holocene*, **24**, 591–602.

Kastens, K.A. and **Cita, M.B.** (1981) Tsunami-induced sediment transport in the abyssal Mediterranean Sea. *GSA Bull.*, **92**, 845–857.

Küchler-Krischun, J. and **Kleiner, J.** (1990) Heterogeneously nucleated calcite precipitation in Lake Constance. A short time resolution study. *Aquat. Sci.*, **52**, 176–197.

Kylander, M.E., **Ampel, L.**, **Wohlfarth, B.** and **Veres, D.** (2011) High-resolution X-ray fluorescence core scanning analysis of Les Echets (France) sedimentary sequence: new insights from chemical proxies. *J. Quat. Sci.*, **26**, 109–117.

Lauterbach, S., **Chapron, E.**, **Brauer, A.**, **Hüls, M.**, **Gilli, A.**, **Arnaud, F.**, **Piccin, A.**, **Nomade, J.**, **Desmet, M.** and **von Grafenstein, U.** (2012) A sedimentary record of Holocene surface runoff events and earthquake activity from Lake Iseo (Southern Alps, Italy). *Holocene*, **22**, 749–760.

Livio, F.A., **Berlusconi, A.**, **Michetti, A.M.**, **Sileo, G.**, **Zerboni, A.**, **Trombino, L.**, **Cremaschi, M.**, **Mueller, K.**, **Vittori, E.**, **Carcano, C.** and **Rogledi, S.** (2009) Active fault-related folding in the epicentral area of the December 25, 1222 (Io=IX MCS) Brescia earthquake (Northern Italy): seismotectonic implications. *Tectonophysics*, **476**, 320–335.

Luino, F., **Belloni, A.**, **Padovan, N.**, **Bassi, M.**, **Bossuto, P.** and **Fassi, P.** (2002) Historical and geomorphological analysis as a research tool for the identification of flood-prone zones and its role in the revision of town planning: the Oglio basin (Valcamonica–Northern Italy). In: *9th Congress of the International Association for Engineering Geology and the Environment, edited by: Van Rooy, JL and Jermy, CA, Durban (South Africa)*, 16–20.

Marziani, G. and **Citterio, S.** (1999) The effects of human impact on the arboreal vegetation near ancient iron smelting sites in Val Gabbia, northern Italy. *Veg. Hist. Archaeobot.*, **8**, 225–229.

Pagani, M., **Garcia-Pelaez, J.**, **Gee, R.**, **Johnson, K.**, **Poggi, V.**, **Styron, R.**, **Weatherill, G.**, **Simionato, M.**, **Viganò, D.** and **Danciu, L.** (2018) Global Earthquake Model (GEM) Seismic Hazard Map (version 2018.1–December 2018). https://doi.org/10.13117/GEM-GLOBAL-SEISMIC-HAZARD-MAP-2018.1

Pilotti, M., **Valerio, G.** and **Leoni, B.** (2013) Data set for hydrodynamic lake model calibration: a deep prealpine case. *Water Resour. Res.*, **49**, 7159–7163.

Pilotti, M., **Valerio, G.**, **Giardino, C.**, **Bresciani, M.** and **Chapra, S.C.** (2018) Evidence from field measurements and satellite imaging of impact of Earth rotation on Lake Iseo chemistry. *J. Great Lakes Res.*, **44**, 14–25.

Pini, R. (2002) A high-resolution Late-Glacial – Holocene pollen diagram from Pian di Gembro (Central Alps, Northern Italy). *Veg. Hist. Archaeobot.*, **11**, 251–262.

Pini, R., **Ravazzi, C.**, **Aceti, A.**, **Castellano, L.**, **Perego, R.**, **Quirino, T.** and **Vallè, F.** (2016) Ecological changes and human interaction in Valcamonica, the Rock Art Valley, since the last deglaciation. *Alp. Mediterr. Quat.*, **29**, 19–34.

Ramisch, F., **Dittrich, M.**, **Mattenberger, C.**, **Wehrli, B.** and **Wüest, A.** (1999) Calcite dissolution in two deep eutrophic lakes. *Geochim. Cosmochim. Acta*, **63**, 3349–3356.

Rapuc, W., **Bouchez, J.**, **Sabatier, P.**, **Genuite, K.**, **Poulenard, J.**, **Gaillardet, J.** and **Arnaud, F.** (2021a) Quantitative evaluation of human and climate forcing on erosion in the alpine Critical Zone over the last 2000 years. *Quat. Sci. Rev.*, **268**, 107127.

Rapuc, W., **Sabatier, P.**, **Andrič, M.**, **Crouzet, C.**, **Arnaud, F.**, **Chapron, E.**, **Šmuc, A.**, **Develle, A.-L.**, **Wilhelm, B.** and **Demory, F.** (2018) 6600 years of earthquake record in the Julian Alps (Lake Bohinj, Slovenia). *Sedimentology*, **65**, 1777–1799.

Rapuc, W., **Sabatier, P.**, **Arnaud, F.**, **Palumbo, A.**, **Develle, A.-L.**, **Reyss, J.-L.**, **Augustin, L.**, **Régnier, E.**, **Piccin, A.**, **Chapron, E.**, **Dumoulin, J.-P.** and **von Grafenstein, U.** (2019) Holocene-long record of flood frequency in the Southern Alps (Lake Iseo, Italy) under human and climate forcing. *Glob. Planet. Change*, **175**, 160–172.

Rapuc, W., **Sabatier, P.** and **Arnaud, F.** (2021b) Human activities disturb lake-sediment records of past flood frequencies. *Past Glob. Changes Mag.*, **29**, 42–43.

Ravazzi, C., **Marchetti, M.**, **Zanon, M.**, **Perego, R.**, **Quirino, T.**, **Deaddis, M.**, **De Amicis, M.** and **Margaritora, D.** (2013) Lake evolution and landscape history in the lower Mincio River valley, unravelling drainage changes in the central Po Plain (N-Italy) since the Bronze Age. *Quat. Int.*, **288**, 195–205.

Regattieri, E., **Zanchetta, G.**, **Isola, I.**, **Zanella, E.**, **Drysdale, R.N.**, **Hellstrom, J.C.**, **Zerboni, A.**, **Dallai, L.**, **Tema, E.**, **Lanci, L.**, **Costa, E.** and **Magrì, F.** (2019) Holocene Critical Zone dynamics in an Alpine catchment inferred from a speleothem multiproxy record: disentangling climate and human influences. *Sci. Rep.*, **9**, 17829.

Reimer, P.J., **Austin, W.E.N.**, **Bard, E.**, **Bayliss, A.**, **Blackwell, P.G.**, **Bronk Ramsey, C.**, **Butzin, M.**, **Cheng, H.**, **Edwards, R.L.**, **Friedrich, M.**, **Grootes, P.M.**, **Guilderson, T.P.**, **Hajdas, I.**, **Heaton, T.J.**, **Hogg, A.G.**, **Hughen, K.A.**, **Kromer, B.**, **Manning, S.W.**, **Muscheler, R.**, **Palmer, J.G.**, **Pearson, C.**, **van der Plicht, J.**, **Reimer, R.W.**, **Richards, D.A.**, **Scott, E.M.**, **Southon, J.R.**, **Turney, C.S.M.**, **Wacker, L.**, **Adolphi, F.**, **Büntgen, U.**, **Capano, M.**, **Fahrni, S.M.**, **Fogtmann-Schulz, A.**, **Friedrich, R.**, **Köhler, P.**, **Kudsk, S.**, **Miyake, F.**, **Olsen, J.**, **Reinig, F.**, **Sakamoto, M.**, **Sookdeo, A.** and **Talamo, S.** (2020) The IntCal20 Northern Hemisphere Radiocarbon Age Calibration Curve (0–55 cal kBP). *Radiocarbon*, **62**, 725–757.

Reyss, J.-L., **Schmidt, S.**, **Legeleux, F.** and **Bonté, P.** (1995) Large, low background well-type detectors for measurements of environmental radioactivity. *Nucl. Instrum. Methods Phys. Res. A*, **357**, 391–397.

Rossato, S., **Fontana, A.** and **Mozzi, P.** (2015) Meta-analysis of a Holocene 14C database for the detection of paleohydrological crisis in the Venetian-Friulian Plain (NE Italy). *Catena*, **130**, 34–45.

Rovida, A.N., **Locati, M.**, **Camassi, R.D.**, **Lolli, B.** & **Gasperini, P.** (2019) Catalogo Parametrico dei Terremoti

Italiani CPTI15, versione 2.0. Istituto Nazionale di Geofisica e Vulcanologia (INGV). https://doi.org/10.13127/CPTI/CPTI15.2

Rovida, A., **Locati, M.**, **Camassi, R.**, **Lolli, B.** and **Gasperini, P.** (2020) The Italian earthquake catalogue CPTI15. *Bull. Earthq. Eng.*, **18**, 2953–2984.

Ruggiero, M.G. and **Poggiani Keller, R.** (2014) *Il Progetto "Monitoraggio e buone pratiche di tutela del patrimonio del sito UNESCO m.94 Arte rupestre della Valle Camonica*. Sestante, Ranica, 344 pp.

Sabatier, P., **Dezileau, L.**, **Briqueu, L.**, **Colin, C.** and **Siani, G.** (2010) Clay minerals and geochemistry record from northwest Mediterranean coastal lagoon sequence: implications for paleostorm reconstruction. *Sediment. Geol.*, **228**, 205–217.

Sabatier, P., **Wilhelm, B.**, **Ficetola, G.F.**, **Moiroux, F.**, **Poulenard, J.**, **Develle, A.-L.**, **Bichet, A.**, **Chen, W.**, **Pignol, C.**, **Reyss, J.-L.**, **Gielly, L.**, **Bajard, M.**, **Perrette, Y.**, **Malet, E.**, **Taberlet, P.** and **Arnaud, F.** (2017) 6-kyr record of flood frequency and intensity in the western Mediterranean Alps – interplay of solar and temperature forcing. *Quat. Sci. Rev.*, **170**, 121–135.

Salmaso, N., **Mosello, R.**, **Garibaldi, L.**, **Decet, F.**, **Brizzio, M.C.** and **Cordella, P.** (2003) Vertical mixing as a determinant of trophic status in deep lakes: a case study from two lakes south of the Alps (Lake Garda and Lake Iseo). *J. Limnol.*, **62**, 33.

Sauerbrey, M.A., **Juschus, O.**, **Gebhardt, A.C.**, **Wennrich, V.**, **Nowaczyk, N.R.** and **Melles, M.** (2013) Mass movement deposits in the 3.6 Ma sediment record of Lake El'gygytgyn. *Far East Russian Arctic. Clim. Past*, **9**, 1949–1967.

Scotti, R., **Brardinoni, F.**, **Alberti, S.**, **Frattini, P.** and **Crosta, G.B.** (2013) A regional inventory of rock glaciers and protalus ramparts in the central Italian Alps. *Geomorphology*, **186**, 136–149.

Serpelloni, E., **Anzidei, M.**, **Baldi, P.**, **Casula, G.** and **Galvani, A.** (2005) Crustal velocity and strain-rate fields in Italy and surrounding regions: new results from the analysis of permanent and non-permanent GPS networks. *Geophys. J. Int.*, **161**, 861–880.

Silva-Sánchez, N., **Martínez Cortizas, A.** and **López-Merino, L.** (2014) Linking forest cover, soil erosion and mire hydrology to late-Holocene human activity and climate in NW Spain. *Holocene*, **24**, 714–725.

Simonneau, A., **Doyen, E.**, **Chapron, E.**, **Millet, L.**, **Vannière, B.**, **Di Giovanni, C.**, **Bossard, N.**, **Tachikawa, K.**, **Bard, E.**, **Albéric, P.**, **Desmet, M.**, **Roux, G.**, **Lajeunesse, P.**, **Berger, J.F.** and **Arnaud, F.** (2013) Holocene land-use evolution and associated soil erosion in the French Prealps inferred from Lake Paladru sediments and archaeological evidences. *J. Archaeol. Sci.*, **40**, 1636–1645.

Strasser, M., **Monecke, K.**, **Schnellmann, M.** and **Anselmetti, F.S.** (2013) Lake sediments as natural seismographs: a compiled record of Late Quaternary earthquakes in Central Switzerland and its implication for Alpine deformation. *Sedimentology*, **60**, 319–341.

Stucchi, M., **Meletti, C.**, **Montaldo, V.**, **Akinci, A.**, **Faccioli, E.**, **Gasperini, P.**, **Malagnini, L.** & **Valensise, G.** (2004) Pericolosità sismica di riferimento per il territorio nazionale MPS04. Istituto Nazionale di Geofisica e Vulcanologia (INGV). https://doi.org/10.13127/sh/mps04/ag

Sturm, M. and **Matter, A.** (1978) Turbidites and Varves in Lake Brienz (Switzerland): Deposition of Clastic Detritus by Density Currents. *Modern and Ancient Lake Sediments*. Wiley Online Library, Hoboken, USA.

Vannière, B., **Magny, M.**, **Joannin, S.**, **Simonneau, A.**, **Wirth, S.B.**, **Hamann, Y.**, **Chapron, E.**, **Gilli, A.**, **Desmet, M.** and **Anselmetti, F.S.** (2013) Orbital changes, variation in solar activity and increased anthropogenic activities: controls on the Holocene flood frequency in the Lake Ledro area, Northern Italy. *Clim. Past*, **9**, 1193–1209.

Verdecchia, A., **Pace, B.**, **Visini, F.**, **Scotti, O.**, **Peruzza, L.** and **Benedetti, L.** (2018) The role of viscoelastic stress transfer in long-term earthquake cascades: insights after the central Italy 2016–2017 seismic sequence. *Tectonics*, **37**, 3411–3428.

Wagner, B., **Reicherter, K.**, **Daut, G.**, **Wessels, M.**, **Matzinger, A.**, **Schwalb, A.**, **Spirkovski, Z.** and **Sanxhaku, M.** (2008) The potential of Lake Ohrid for long-term palaeoenvironmental reconstructions. *Palaeogeogr. Palaeoclimatol. Palaeoecol.*, **259**, 341–356.

Walsh, K., **Berger, J.-F.**, **Roberts, C.N.**, **Vanniere, B.**, **Ghilardi, M.**, **Brown, A.G.**, **Woodbridge, J.**, **Lespez, L.**, **Estrany, J.**, **Glais, A.**, **Palmisano, A.**, **Finné, M.** and **Verstraeten, G.** (2019) Holocene demographic fluctuations, climate and erosion in the Mediterranean: a meta data-analysis. *Holocene*, **29**, 864–885.

Wang, J., **Howarth, J.D.**, **McClymont, E.L.**, **Densmore, A.L.**, **Fitzsimons, S.J.**, **Croissant, T.**, **Gröcke, D.R.**, **West, M.D.**, **Harvey, E.L.**, **Frith, N.V.**, **Garnett, M.H.** and **Hilton, R.G.** (2020) Long-term patterns of hillslope erosion by earthquake-induced landslides shape mountain landscapes. *Sci. Adv.*, **6**, eaaz6446.

Wessels, M. (1998) Natural environmental changes indicated by Late Glacial and Holocene sediments from Lake Constance. *Germany. Palaeogeogr. Palaeoclimatol. Palaeoecol.*, **140**, 421–432.

Wiemer, S., **Kraft, T.** and **Landtwing, D.S.** (2015) Seismic Risk. *Energy from the Earth: Deep geothermal as a resource for the future? TA Swiss Geothermal Project Final Report*, pp. 263–295. Paul Scherrer Institute, Villingen.

Wilhelm, B., **Arnaud, F.**, **Sabatier, P.**, **Magand, O.**, **Chapron, E.**, **Courp, T.**, **Tachikawa, K.**, **Fanget, B.**, **Malet, E.**, **Pignol, C.**, **Bard, E.** and **Delannoy, J.J.** (2013) Palaeoflood activity and climate change over the last 1400 years recorded by lake sediments in the north-west European Alps. *J. Quat. Sci.*, **28**, 189–199.

Wilhelm, B., **Nomade, J.**, **Crouzet, C.**, **Litty, C.**, **Sabatier, P.**, **Belle, S.**, **Rolland, Y.**, **Revel, M.**, **Courboulex, F.**, **Arnaud, F.** and **Anselmetti, F.S.** (2016) Quantified sensitivity of small lake sediments to record historic earthquakes: implications for paleoseismology. *J. Geophys. Res. Earth Surf.*, **121**, 2–16.

Wirth, S.B., **Gilli, A.**, **Simonneau, A.**, **Ariztegui, D.**, **Vannière, B.**, **Glur, L.**, **Chapron, E.**, **Magny, M.** and **Anselmetti, F.S.** (2013a) A 2000 year long seasonal record of floods in the southern European Alps. *Geophys. Res. Lett.*, **40**, 4025–4029.

Wirth, S.B., **Glur, L.**, **Gilli, A.** and **Anselmetti, F.S.** (2013b) Holocene flood frequency across the Central Alps–solar forcing and evidence for variations in North Atlantic atmospheric circulation. *Quat. Sci. Rev.*, **80**, 112–128.

Zádorová, T., **Penížek, V.**, **Šefrna, L.**, **Drábek, O.**, **Mihaljevič, M.**, **Volf, Š.** and **Chuman, T.** (2013) Identification of Neolithic to Modern erosion–sedimentation phases using geochemical approach in a loess covered sub-catchment of South Moravia, Czech Republic. *Geoderma*, **195–196**, 56–69.

Manuscript received 28 January 2021; revision accepted 11 January 2022

Supporting Information

Additional information may be found in the online version of this article:

Figure S1. Coring technical scheme for SEB18_I sediment section.

Figure S2. Factor map from a hierarchical clustering on principal component analysis (HCPC) realized on the layers presenting a detrital composition (low Ca/Sr_{mean} values) and Zr/K_{max} values higher than the values of the continuous sedimentation.

Table S1. Age, depth, thickness, Zr/K_{max}, Ca/Sr_{mean} values and associated cluster from the HCPC for layers.

Data S1. Coring technical scheme for SEB18_I sediment section.

Data S2. Statistical classification to distinguish homogenite and turbidite-type deposits.